ACS NANO
Cite This: ACS Nano 2019, 13, 10939−10960
www.acsnano.org

ARTICLE

Mucosal Immunization with a pH-Responsive Nanoparticle Vaccine Induces Protective CD8$^+$ Lung-Resident Memory T Cells

Frances C. Knight,[†] Pavlo Gilchuk,[‡,§,∥] Amrendra Kumar,[‡,∥] Kyle W. Becker,[⊥] Sema Sevimli,[⊥] Max E. Jacobson,[⊥] Naveenchandra Suryadevara,[‡,∥] Lihong Wang-Bishop,[⊥] Kelli L. Boyd,[‡,#] James E. Crowe, Jr.,[‡,§,#,¶,△,▼,○] Sebastian Joyce,[‡,∥,#,○] and John T. Wilson*[,†,⊥,#,○,■]

[†]Department of Biomedical Engineering, Vanderbilt University, Nashville, Tennessee 37235, United States
[‡]Department of Pathology, Microbiology, and Immunology, Vanderbilt University Medical Center, Nashville, Tennessee 37232, United States
[§]Vanderbilt Vaccine Center, Vanderbilt University Medical Center, Nashville, Tennessee 37232, United States
[∥]Department of Veterans Affairs Tennessee Valley Healthcare System, Nashville, Tennessee 37212, United States
[⊥]Department of Chemical and Biomolecular Engineering, Vanderbilt University, Nashville, Tennessee 37235, United States
[#]Vanderbilt Institute for Infection, Immunology, and Inflammation, Vanderbilt University Medical Center, Nashville, Tennessee 37232, United States
[¶]Department of Pediatrics, Vanderbilt University Medical Center, Nashville, Tennessee 37232, United States
[△]Chemical and Physical Biology Program, Vanderbilt University, Nashville, Tennessee 37235, United States
[▼]Department of Cell and Developmental Biology, Vanderbilt University, Nashville, Tennessee 37235, United States
[○]Vanderbilt Center for Immunobiology, Vanderbilt University Medical Center, Nashville, Tennessee 37232, United States
[■]Vanderbilt-Ingram Cancer Center, Vanderbilt University Medical Center, Nashville, Tennessee 37232, United States

S *Supporting Information*

ABSTRACT: **Tissue-resident memory T cells (T_{RM}) patrol nonlymphoid organs and provide superior protection against pathogens that commonly infect mucosal and barrier tissues, such as the lungs, intestine, liver, and skin. Thus, there is a need for vaccine technologies that can induce a robust, protective T_{RM} response in these tissues. Nanoparticle (NP) vaccines offer important advantages over conventional vaccines; however, there has been minimal investigation into the design of NP-based vaccines for eliciting T_{RM} responses. Here, we describe a pH-responsive polymeric nanoparticle vaccine for generating antigen-specific CD8$^+$ T_{RM} cells in the lungs. With a single intranasal dose, the NP vaccine elicited airway- and lung-resident CD8$^+$ T_{RM} cells and protected against respiratory virus challenge in both sublethal (vaccinia) and lethal (influenza) infection models for up to 9 weeks after immunization. In elucidating the contribution of material properties to the resulting T_{RM} response, we found that the pH-responsive activity of the carrier was important, as a structurally analogous non-pH-responsive control carrier elicited significantly fewer lung-resident CD8$^+$ T cells. We also demonstrated that dual-delivery of protein antigen and nucleic acid adjuvant on the same NP substantially enhanced the magnitude, functionality, and longevity of the antigen-specific CD8$^+$ T_{RM} response in the lungs. Compared to administration of soluble antigen and adjuvant, the NP also mediated retention of vaccine cargo in pulmonary antigen-presenting cells (APCs), enhanced APC activation, and increased production of T_{RM}-related cytokines. Overall, these data suggest a promising vaccine platform technology for rapid generation of protective CD8$^+$ T_{RM} cells in the lungs.**

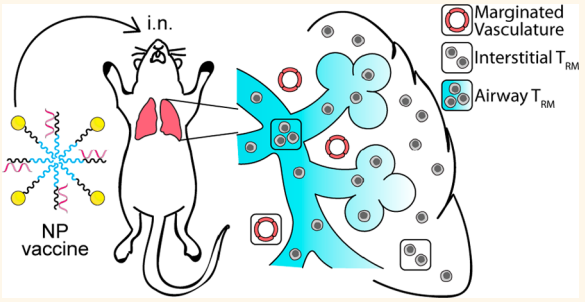

KEYWORDS: *nanoparticle, subunit vaccine, nucleic acid adjuvant, intranasal, lungs, tissue-resident memory T cells, influenza*

Tissue-resident memory T cells (T_{RM}) are a specialized subset of memory cells with a distinct phenotype that reside in nonlymphoid tissues and act as a first line of defense against many pathogens.[1−3] T_{RM} cells remain localized

Received: January 13, 2019
Accepted: September 25, 2019
Published: September 25, 2019

DOI: 10.1021/acsnano.9b00326
ACS Nano 2019, 13, 10939−10960

in their home tissues due to a combination of adhesion molecules and a lack of homing mechanisms for trafficking to distal lymphoid organs or circulating in the blood. As such, they are optimally positioned to respond more quickly than peripheral memory T cells. T_{RM} have been identified in several organs, including the skin, liver, kidneys, brain, and mucosal tissues such as the lungs, intestine, and female reproductive tract.[4,5] These cells play a key role in protection against multiple infectious diseases for which new or improved vaccines are needed, such as influenza, tuberculosis, respiratory syncytial virus, and HIV/AIDS.[6−9] T_{RM} are also important in immunity against tumors, including breast cancer, melanoma, and lung cancer.[10−13] For several diseases, antibodies or nonresident memory T cells alone are not sufficient for optimal protection;[14−17] however, very few currently approved vaccines have been shown to generate T_{RM} cells.[18,19] Therefore, there is a critical need to develop new vaccines that can induce protective T_{RM} in target tissues.

Pulmonary T_{RM} reside in both the lung interstitium and airways[20,21] and are critical in mediating protection against respiratory pathogens.[18,19,22] Mucosal vaccination has garnered attention as a superior route of immunization over traditional intramuscular injections for several reasons, including its ability to mimic routes of pathogen entry and generate tissue-specific immune cells optimally positioned to fight off future infection.[13,23] Specifically, pulmonary immunization *via* intranasal (i.n.) administration is advantageous for generating T_{RM} in the lungs.[24,25] Additionally, there is evidence that pulmonary immunization can generate T cell responses in distal mucosal tissues.[26] Hence, the development of vaccine formulations that can be administered by mucosal routes holds great promise for a new generation of T_{RM}-targeted vaccines.

Protein-based subunit vaccines have been widely studied as a next-generation vaccine platform, including in the context of mucosal delivery.[27] A major drawback of subunit vaccines, however, is poor immunogenicity due to several drug delivery barriers, including rapid antigen clearance with poor uptake by dendritic cells and minimal accumulation in draining lymph nodes. Subunit vaccines are particularly inept at eliciting $CD8^+$ T cells, which are required for immunity against many pathogens and cancers.[28,29] Eliciting a robust $CD8^+$ T cell response requires antigen presentation on major histocompatibility complex class I (MHC-I) by dendritic cells (DCs) in the context of additional molecular cues (co-stimulation, cytokines) that drive $CD8^+$ T cell expansion and differentiation.[28,30] To achieve presentation by MHC-I, administered antigen must either be endocytosed by specialized cross-presenting DC subsets or delivered to the classical cytosolic MHC-I antigen processing pathway. However, the predominant fate of soluble endocytosed antigen is lysosomal degradation, with minimal presentation on MHC-I.[31,32]

Despite their limited capacity to generate $CD8^+$ T cells, the superior safety profile of subunit vaccines has motivated strategies to improve their efficacy.[33] Toward this end, a variety of nanoparticle (NP)-based vaccine delivery systems have been developed that utilize material properties to enhance antigen uptake by DCs, promote antigen cross-presentation, and/or co-deliver immunostimulatory adjuvants in order to potentiate $CD8^+$ T cell responses to immunization.[34−39] This includes NP formulations that have been administered i.n. to generate pulmonary T cell responses in mouse models of infection and cancer.[40−42] However, to date, only a few reports have evaluated the ability of NP-based subunit vaccines to specifically induce $CD8^+$ T_{RM} cells in the lungs.[26,43,44] Moreover, whereas NP design principles for eliciting robust systemic T cell responses have largely been established, the ways in which properties of NP vaccines can be engineered to augment T_{RM} responses elicited by mucosal immunization have not been explored. This motivates the need for the design, optimization, and evaluation of NP vaccines for installing this unique memory T cell population in the lungs and other mucosal tissues.

Although elucidation of the mechanisms underlying induction and maintenance of $CD8^+$ T_{RM} in the lungs remains an active area of investigation, lessons in vaccine design can be taken from studies of respiratory viral infections like influenza, in which robust and durable T_{RM} are often generated.[17,45] These studies motivate the design of NP vaccines that can mimic viral infection by enhancing antigen uptake and cross-presentation in APCs, allowing for co-delivery of antigen and adjuvant, and/or increasing local antigen persistence in tissues.[46−49] Therefore, in this study, we leveraged a viral-mimetic polymeric NP vaccine delivery system that utilizes a pH-dependent endosomal escape mechanism to release cargo into the cytosol, resulting in enhanced antigen delivery to the MHC-I processing pathway.[37] Additionally, the corona of the NP is designed to enable dual-delivery of antigen and nucleic acid adjuvant on the same particle, further augmenting its ability to mimic pathogen encounter and enhance the $CD8^+$ T cell response.

Here, we demonstrate that a pH-responsive NP vaccine dual-loaded with ovalbumin protein antigen (OVA) and CpG DNA adjuvant enhanced the magnitude, functionality, and longevity of the pulmonary $CD8^+$ T_{RM} response in mice. It also improved activation of pulmonary APCs and promoted antigen persistence in the lungs. Importantly, a single i.n. dose of the NP vaccine conferred protection against respiratory challenge with a recombinant vaccinia virus containing the $CD8^+$ T cell epitope of OVA. Of significance to the design of T_{RM}-targeted NP vaccines, we also show that the pH-responsive activity of the NP is important for induction of lung-resident $CD8^+$ T cells, demonstrating that a material property can be harnessed to install this important cell population in a mucosal tissue. Finally, we show that a clinically relevant antigen, influenza A virus nucleoprotein, can be delivered *via* the NP vaccine, generate a $CD8^+$ T_{RM} response in the lungs, and confer protection in a lethal respiratory influenza virus challenge model after a single dose. Collectively, our results suggest a promising experimental vaccine platform for generating $CD8^+$ T_{RM} against respiratory infections and offer evidence that NP properties can be modulated to augment T_{RM} responses elicited by pulmonary immunization.

RESULTS AND DISCUSSION

Intranasal Antigen Delivery with a pH-Responsive Nanoparticle Carrier Enhances the Lung-Resident $CD8^+$ T Cell Response. The nanoparticle described in this report is formulated using a pH-responsive diblock copolymer designed to enhance cytosolic delivery of vaccine cargo and strengthen the $CD8^+$ T cell response by promoting processing and presentation of antigen in the MHC-I pathway.[37] The polymer is composed of two functional blocks synthesized by reversible addition−fragmentation chain transfer (RAFT) polymerization (Scheme S1A,B). The first block is a hydrophilic copolymer of dimethylaminoethyl methacrylate (DMAEMA) and pyridyl disulfide ethyl methacrylate (PDSMA). PDSMA provides pyridyl disulfide groups on the surface of the particle for conjugation to thiolated protein antigen, and DMAEMA

DOI: 10.1021/acsnano.9b00326
ACS Nano 2019, 13, 10939−10960

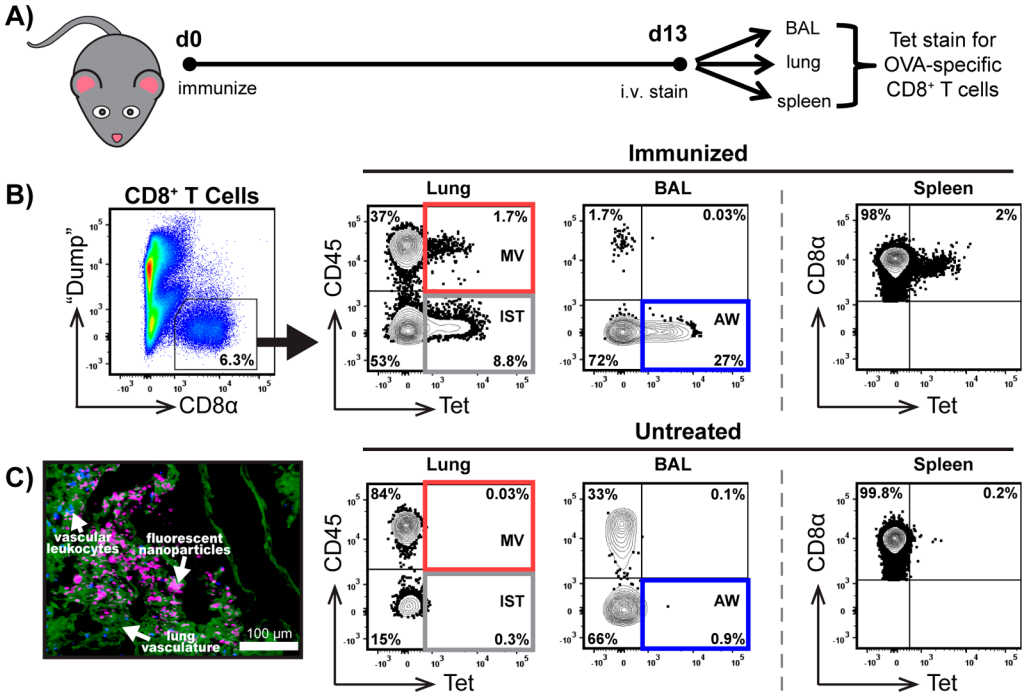

Figure 1. Intravascular staining is used to determine localization of CD8⁺ T cells after intranasal delivery to the lungs. (A) Schematic of the experimental timeline. (B) Flow cytometry was used to identify antigen-specific (Tet⁺) CD8⁺ T cells in distinct lung compartments (airway, AW; interstitium, IST; marginated vasculature, MV) and the spleen. BAL was collected to discriminate AW *vs* IST cells, and i.v. staining with αCD45 antibody discriminated IST (CD45⁻) *vs* MV (CD45⁺) cells. Samples were stained with PE-labeled SIINFEKL/MHC-I tetramer to identify antigen-specific CD8⁺ T cells. After gating out CD11b⁺, CD11c⁺, B220⁺, and CD4⁺ cells ("dump"), CD8α⁺CD45⁻Tet⁺ events in AW and IST, CD8α⁺CD45⁺Tet⁺ events in MV, and CD8α⁺Tet⁺ events in the spleen were quantified. Dot plots are representative of the gating strategy used in multiple experiments (see Figure S3A–C). (C) In conjunction with i.v. staining, microscopy was used to visualize fluorescent OVA–NP conjugates in the lower airways 24 h after immunization. Lungs were stained with αCD45 antibody, which labels vascular leukocytes, and tomato lectin, which binds to capillary endothelial cells and allows for visualization of lung structure. Purple, OVA–NP; blue, vascular leukocytes; green, lung vasculature. Scale bar = 100 μm. Immunization dose: 25 μg NP, 7.5 μg OVA.

contributes cationic charge for electrostatic complexation with a nucleic acid adjuvant. The second block is a pH-responsive, endosomolytic copolymer of propylacrylic acid (PAA), butyl methacrylate (BMA), and DMAEMA, which drives micellar nanoparticle assembly due to its hydrophobic nature. After cellular uptake and in response to endosomal acidification, the micellar structure of the NP transforms to expose the membrane-destabilizing core (PAA-*co*-BMA-*co*-DMAEMA), which promotes endosomal escape and cytosolic antigen delivery to the MHC-I pathway.

Although this mechanism of NP-mediated antigen cross-presentation has been utilized to enhance the splenic CD8⁺ T cell response *via* subcutaneous administration, it is unknown whether pH-responsive activity can be leveraged to generate a lung-resident CD8⁺ T cell response after intranasal antigen delivery. To evaluate this, both pH-responsive NP and nonresponsive control NP (second block consisting only of BMA) were synthesized and characterized (Scheme S1A–C, Table S1, and Figure S1), and a model protein antigen, ovalbumin (OVA), was thiolated and covalently conjugated to both NP carriers (Figure S2A,C). Mice were immunized i.n. with antigen–NP conjugates made using either pH-responsive nanoparticles (OVA–NP_{pH}) or control nanoparticles (OVA–NP_{ctrl}). On day 13 after immunization, mice were injected intravenously (i.v.) with αCD45 antibody to distinguish CD45⁺ blood-borne cells in the lung vasculature ("marginated vasculature", MV) from tissue-resident CD45⁻ cells in the lung interstitium (IST). By directly discriminating between cells residing in distinct lung compartments, this intravascular staining technique provides an accurate and robust method for establishing tissue residence.[9,50–52] Broncheoalveolar lavage fluid (BAL) was also collected to differentiate CD45⁻ cells resident in the airways (AW) from CD45⁻ IST-resident cells[52] (Figure 1A).

Cells obtained from lungs, BAL, and spleens were stained with fluorescent antibodies against a panel of surface markers and with fluorescent MHC-I tetramer (Tet) containing SIINFEKL peptide (the immunodominant H-2K^b epitope for OVA). Samples were then analyzed by flow cytometry to quantify antigen-specific CD8⁺ T cells (Tet⁺CD8α⁺CD11b⁻CD11c⁻B220⁻CD4⁻) in each lung compartment and the spleen (Figures 1B and S3A–C). Fluorescence microscopy was also used to confirm that OVA–NP conjugates reached the lower airways after i.n. administration. Conjugates formulated with Alexa Fluor 647-labeled OVA were visible in lungs harvested 24 h after immunization (Figure 1C). We found that the pH-responsive carrier elicited a significantly greater antigen-specific (Tet⁺) CD8⁺ T cell response than the control carrier in the AW (Figure 2A) and IST (Figure 2B), whereas there was no significant difference in the response between carriers in the MV (Figure 2C) and spleen (Figure 2D). These data indicate that the pH-responsive property of the NP is important for generating a tissue-resident CD8⁺ T cell response in the lungs and serve to demonstrate the importance of NP properties in development of T_{RM}-targeted vaccines.

DOI: 10.1021/acsnano.9b00326
ACS Nano 2019, 13, 10939–10960

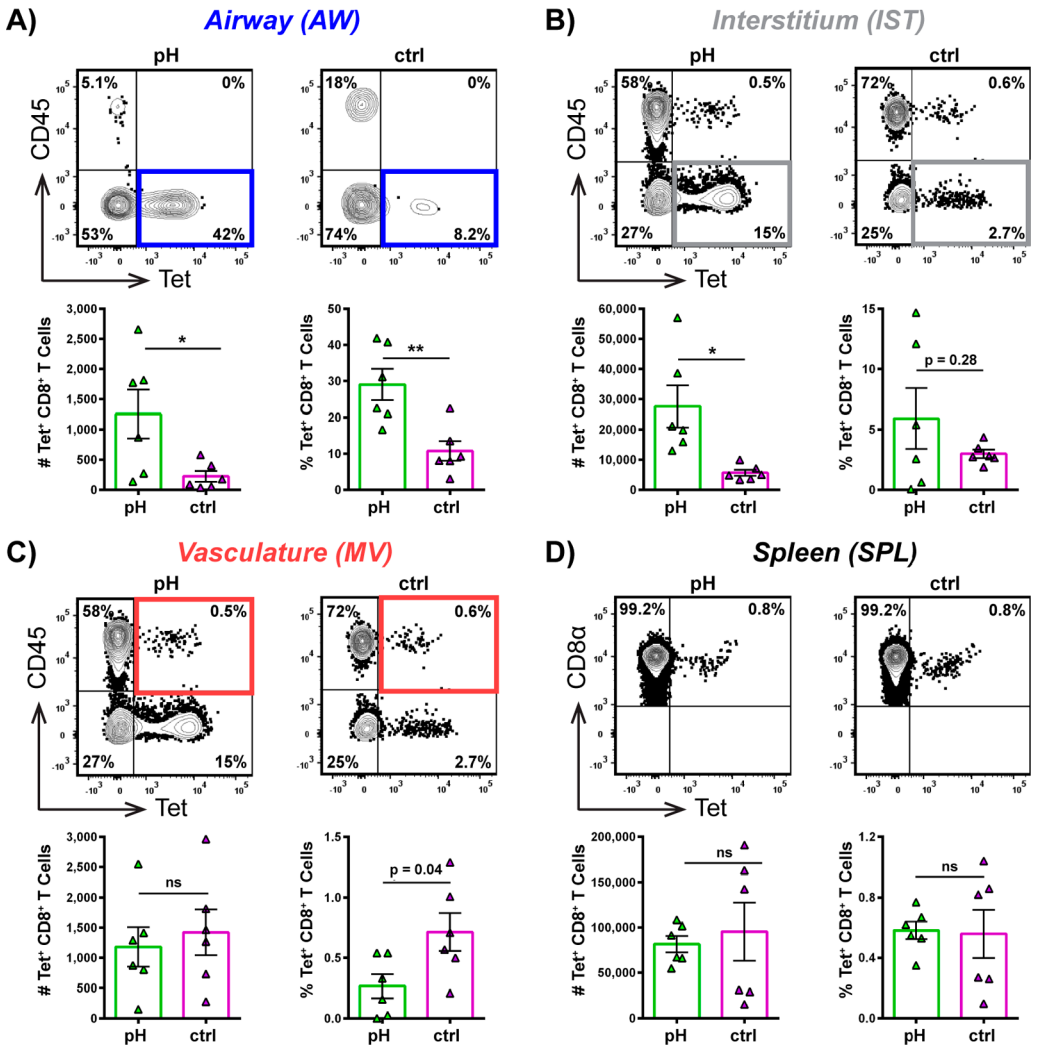

Figure 2. Intranasal antigen delivery with pH-responsive nanoparticles enhances lung-resident CD8$^+$ T cell response. Number (#) and frequency (%) of Tet$^+$ CD8$^+$ T cells in (A) AW, (B) IST, (C) MV, and (D) spleen were enumerated on day 13 after i.n. administration of OVA−NP$_{pH}$ or OVA−NP$_{ctrl}$. Representative dot plots are gated on viable CD8$^+$ T cells. Immunization dose: 25 μg NP, 7.5 μg OVA. Data are mean ± SEM and representative of two independent experiments, with n = 6 per group. Limits of detection: 1 cell (AW), 5 cells (IST/MV), 25 cells (spleen); *p < 0.05, **p < 0.01 by unpaired t test; ns, not significant. See also Figure S3A−C.

Intranasal Dual-Delivery of Antigen and Adjuvant with pH-Responsive Nanoparticles Enhances Magnitude and Functionality of the Lung-Resident CD8$^+$ T Cell Response. After demonstrating the importance of pH-responsiveness in generating a robust lung-resident CD8$^+$ T cell response, we next asked whether dual-delivery of antigen and an immunostimulatory adjuvant on the same pH-responsive NP would further augment this response. Although this pathogen-mimetic property has previously been shown to enhance the systemic CD8$^+$ T cell response,[37] to our knowledge, the importance of NP-mediated dual-delivery for generating tissue-resident CD8$^+$ T cells has not been clearly demonstrated. Therefore, nanoparticles were coloaded with OVA protein and a nucleic acid adjuvant, CpG ODN 1826 (a single-stranded DNA agonist for TLR9). CpG DNA has been shown to enhance the CD8$^+$ T cell response and has precedence for use in pulmonary immunization.[40,44,53] CpG was electrostatically complexed to OVA−NP conjugates (Figure S2B), and this formulation is referred to henceforth as OVA−NP/CpG or the "nanoparticle vaccine".

On day 0, mice were immunized i.n. with OVA−NP/CpG, OVA−NP conjugate, a mixture of soluble OVA+CpG, a mixture of soluble OVA+NP, or NP/CpG complex mixed with soluble OVA (NP/CpG+OVA) (Figure 3A). On day 13 after immunization, mice were injected i.v. with αCD45 antibody and lungs, BAL, and spleens were collected and analyzed by flow cytometry as described above (Figures 1A,B and S3A−C). Mice immunized with a single dose of OVA−NP/CpG produced significantly more Tet$^+$ CD8$^+$ T cells relative to all other formulations (Figure 3B−E). This increased response was observed in both the AW (Figure 3B) and IST (Figure 3C) lung compartments, as well as in the MV (Figure 3D) and spleen (Figure 3E). These data demonstrate that NP-mediated dual-delivery of antigen and adjuvant to the lungs enhances the CD8$^+$ T cell response over immunization with OVA−NP. The effect was particularly prominent in the IST, indicating the ability of the NP vaccine to induce lung-resident CD8$^+$ T cells. Simple mixing of components (OVA+CpG, OVA+NP) was ineffective, and dual-delivery on the same particle was crucial, as the formulation containing all three components without coloading (NP/CpG+OVA) did not induce a robust response.

DOI: 10.1021/acsnano.9b00326
ACS Nano 2019, 13, 10939−10960

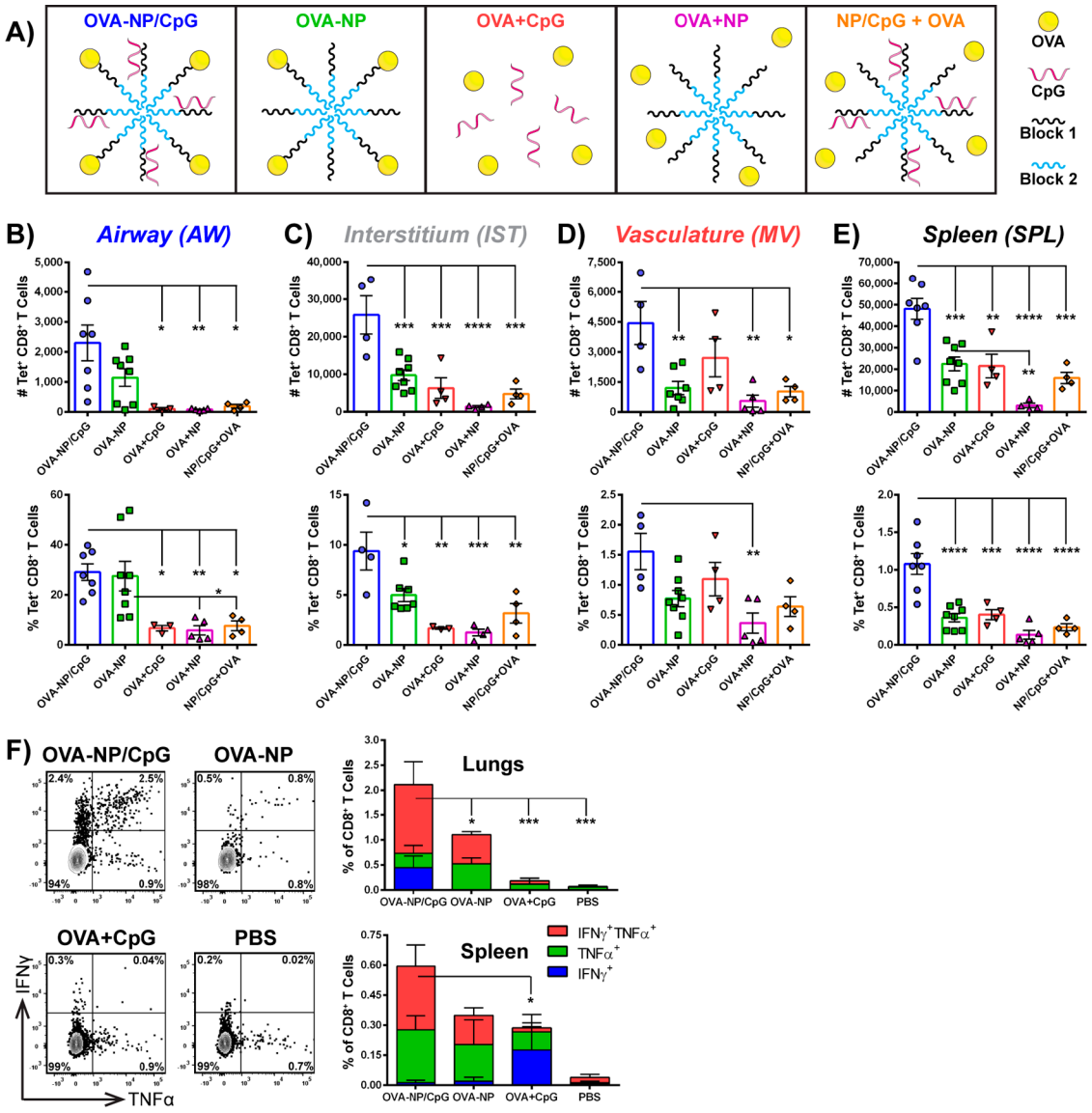

Figure 3. Intranasal dual-delivery of antigen and adjuvant *via* nanoparticle vaccine enhances magnitude and functionality of lung-resident CD8$^+$ T cell response. (A) Mice were immunized on day 0 with the NP vaccine or control formulations, and lungs, spleens, and/or BAL were collected on day 13 for analysis of the immune response by tetramer staining or ICCS. (B–E) Number (#) and frequency (%) of Tet$^+$ CD8$^+$ T cells in (B) AW, (C) IST, (D) MV, and (E) spleen were enumerated on day 13 after i.n. administration of OVA–NP/CpG or control formulations. (F) ICCS was used to identify % CD8$^+$ T cells positive for IFNγ and/or TNFα after *ex vivo* restimulation of lungs and spleen with SIINFEKEL peptide. Statistical differences are shown for the IFNγ^+TNFα^+ group only. Data are mean ± SEM and representative of one to three independent experiments, with (B–E) n = 4–7 per group and (F) n = 2–4 per group. Immunization dose: 25 μg NP, 7.5 μg OVA, 1.4 μg CpG. Limits of detection for (B–E): 1 cell (AW), 5 cells (IST/MV), 25 cells (spleen); *p < 0.05, **p < 0.01, ***p < 0.001, ****p < 0.0001 by (B–E) ordinary one-way ANOVA with Tukey's multiple comparisons test or (F) ordinary two-way ANOVA with Tukey's multiple comparisons test. See also Figure S3A–D.

T cell functionality after immunization was assessed *via* intracellular cytokine staining (ICCS). Mice were immunized on day 0 with OVA–NP/CpG, OVA–NP, OVA+CpG, or PBS, and lungs and spleens were collected on day 13. Lung and spleen cells were restimulated with SIINFEKEL peptide and analyzed by flow cytometry for production of IFNγ and TNFα (Figure S3D). Mice immunized with OVA–NP/CpG had a greater percentage of polyfunctional (IFNγ^+TNFα^+) antigen-specific CD8$^+$ T cells in both the lungs and spleen, relative to all other formulations (Figure 3F). This further supports the importance of antigen and adjuvant dual-delivery in generating a robust and functional CD8$^+$ T cell response, particularly in the lungs.

In addition, the CD8$^+$ T cell response in mice immunized i.n. with OVA–NP/CpG was compared to the response to subcutaneous (s.c.) immunization with the same formulation. It has been reported that systemic administration of antigenic protein and adjuvant *via* the intraperitoneal route generates low numbers of lung-resident CD8$^+$ T cells relative to i.n. administration.[52] We hypothesized that s.c. immunization with the NP vaccine would also be ineffective. On day 13 postimmunization, tetramer staining was used to analyze the antigen-specific CD8$^+$ T cell response to i.n. or s.c. administration of the NP vaccine. Responses in the AW (Figure 4A) and IST (Figure 4B) were significantly higher for mice immunized i.n.; however, there was no difference between

DOI: 10.1021/acsnano.9b00326
ACS Nano 2019, 13, 10939–10960

administration routes for MV (Figure 4C) or spleen (Figure 4D). Consistent with previous reports, this demonstrates the importance of i.n. administration of the NP vaccine for generating a lung-resident CD8$^+$ T cell response.[26,42,43]

Pulmonary toxicity is an important consideration when evaluating the translational potential of mucosal vaccines. NP-based i.n. or intratracheal vaccine and/or CpG administration

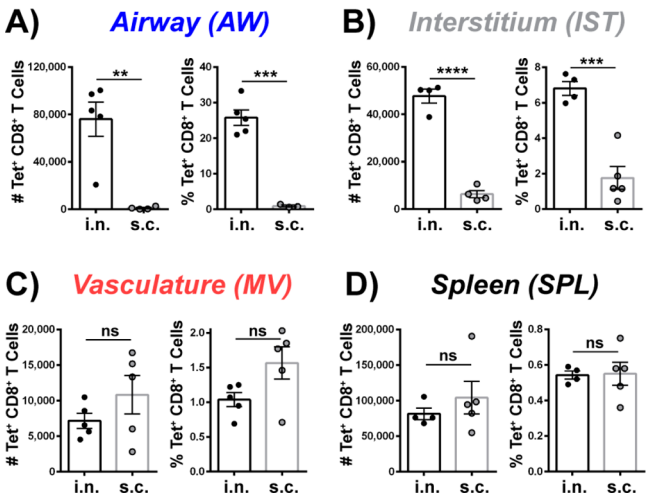

Figure 4. Pulmonary immunization *via* intranasal administration is optimal for generating a lung-resident CD8$^+$ T cell response. Number (#) and frequency (%) of Tet$^+$ CD8$^+$ T cells in (A) AW, (B) IST, (C) MV, and (D) spleen were enumerated on day 13 after i.n. or s.c. administration of OVA−NP/CpG. Data are mean ± SEM, with n = 4−5 per group. Immunization dose: 25 μg NP, 7.5 μg OVA, 1.4 μg CpG. Limits of detection: 1 cell (AW), 5 cells (IST/MV), 25 cells (spleen); **p < 0.01, ***p < 0.001, ****p < 0.0001 by unpaired t test.

have previously been reported to be safe in mice.[26,40,41] In this work, mice immunized i.n. exhibited minimal weight loss within the first 2 days and recovered rapidly (Figure S4A). In addition, lung tissue harvested at day 1 and day 12 after immunization with either OVA−NP/CpG or OVA+CpG was evaluated for immunopathology. Mild inflammation was induced by both formulations, with no signs of pathology or tissue damage, and findings were consistent between animals in the same treatment group (Figure S4B). This mild inflammation was associated with infiltration of immune cells to the lungs (lymphocytes, macrophages, neutrophils at day 1; lymphocytes, plasma cells, macrophages at day 12) and is consistent with flow cytometry data showing recruitment of lymphoid cells in response to i.n. vaccine administration (Figure 3B−E).

Taken together, these data demonstrate that i.n. administration of the NP vaccine is safe and can significantly enhance the magnitude and functionality of the antigen-specific CD8$^+$ T cell response within 13 days and after a single dose. In addition to local lung-resident CD8$^+$ T cells, the NP vaccine can also induce systemic immunity *via* i.n. administration. Importantly, pathogen-mimetic dual-delivery of antigen and adjuvant on the same particle is integral to the magnitude and functionality of this response.

Nanoparticle-Mediated Dual-Delivery Enhances Persistence and Colocalization of Cargo and Expression of Activation Markers in Pulmonary Antigen-Presenting Cells. We next asked what characteristics of the NP vaccine formulation could account for the enhanced lung-resident CD8$^+$ T cell response. Previous reports have demonstrated the importance of antigen persistence in establishing T_{RM} populations in the lungs and other tissues.[2,47,48,54] In addition, cross-presenting CD103$^+$ DCs are involved in activation of precursor T_{RM}, and alveolar macrophages can promote formation of T_{RM} in the lungs.[55−57] We hypothesized that the NP formulation would increase vaccine residence time in the lungs, thereby promoting extended co-delivery of vaccine cargo (OVA and CpG) to pulmonary innate immune cells. We also postulated that this NP-mediated persistence would prolong activation of local APCs, thus leading to an improved downstream adaptive immune response and formation of T_{RM} in the lungs.[48]

To evaluate this, we labeled OVA with Alexa Fluor 647 (OVA_{647}) and CpG with Alexa Fluor 488 (CpG_{488}) and immunized mice i.n. with fluorescent formulations (OVA_{647}−NP/CpG_{488} or OVA_{647}+CpG_{488}) or PBS. First, to assess organ-level local and systemic biodistribution of the formulations, lungs and spleens were harvested at 24, 48, and 72 h postimmunization and imaged to determine whether the NP vaccine enhanced OVA retention relative to the soluble formulation. Quantification of OVA_{647} average radiant efficiency in fluorescent images demonstrated that antigen remained in the lungs longer for mice immunized with the NP vaccine. At both 48 and 72 h postimmunization, mice receiving OVA_{647}−NP/CpG_{488} had significantly more OVA_{647} fluorescence in the lungs relative to OVA_{647}+CpG_{488} (Figure 5A). In addition, there was negligible fluorescence present in spleens at all time points, suggesting that i.n. administration leads to localized pulmonary delivery with minimal systemic distribution.

In addition to assessment of localization and retention at the organ level, lungs were also analyzed by flow cytometry to evaluate uptake of vaccine cargo in pulmonary APC subsets (Figure S5A), as well as expression of the co-stimulatory marker CD86 in these populations. The cell types analyzed were as follows: (1) alveolar macrophages (AMφ), (2) interstitial macrophages (IMφ), (3) CD103$^+$ dendritic cells (CD103$^+$ DC), (4) CD11b$^+$ dendritic cells (CD11b$^+$ DC), (5) a population of monocyte- and macrophage-like cells not encompassed by other subsets (Mono/Mφ), (6) granulocytes (Gran), and (7) "other" (anything not included in previous categories).[58] We expected dual-delivery of OVA_{647} and CpG_{488} with the NP vaccine would increase their colocalization within cells, so we analyzed cells that were double-positive for both cargoes (OVA$^+$CpG$^+$) (Figure S5B). Uptake was quantified for each cell subset as both "cell count" (# OVA$^+$CpG$^+$ events) and "relative uptake" (mean fluorescence intensity (MFI) of either OVA or CpG multiplied by # OVA$^+$CpG$^+$ events). Relative uptake was used to account for both the number of cells containing cargo (#) and the total amount of cargo taken up (MFI).[26] Initially, after 24 h, there was no difference in uptake between OVA−NP/CpG and OVA+CpG (Figures 5B and S5C, top row). Starting at 48 h and increasing by 72 h post-immunization, there was significantly more cargo colocalization from the NP vaccine in several cell types, including CD103$^+$ DCs and CD11b$^+$ DCs at 48 h (Figures 5B and S5C, middle row), and DCs, AMφ, IMφ, Mono/Mφ, and Gran at 72 h (Figures 5B and S5C, bottom row). These data reflect the results obtained from fluorescent organ imaging (Figure 5A) and demonstrate that NP delivery prolongs antigen and adjuvant colocalization and retention in pulmonary APCs, suggesting that an NP-mediated increase in local antigen persistence may contribute to the generation of lung T_{RM}.

DOI: 10.1021/acsnano.9b00326
ACS Nano 2019, 13, 10939−10960

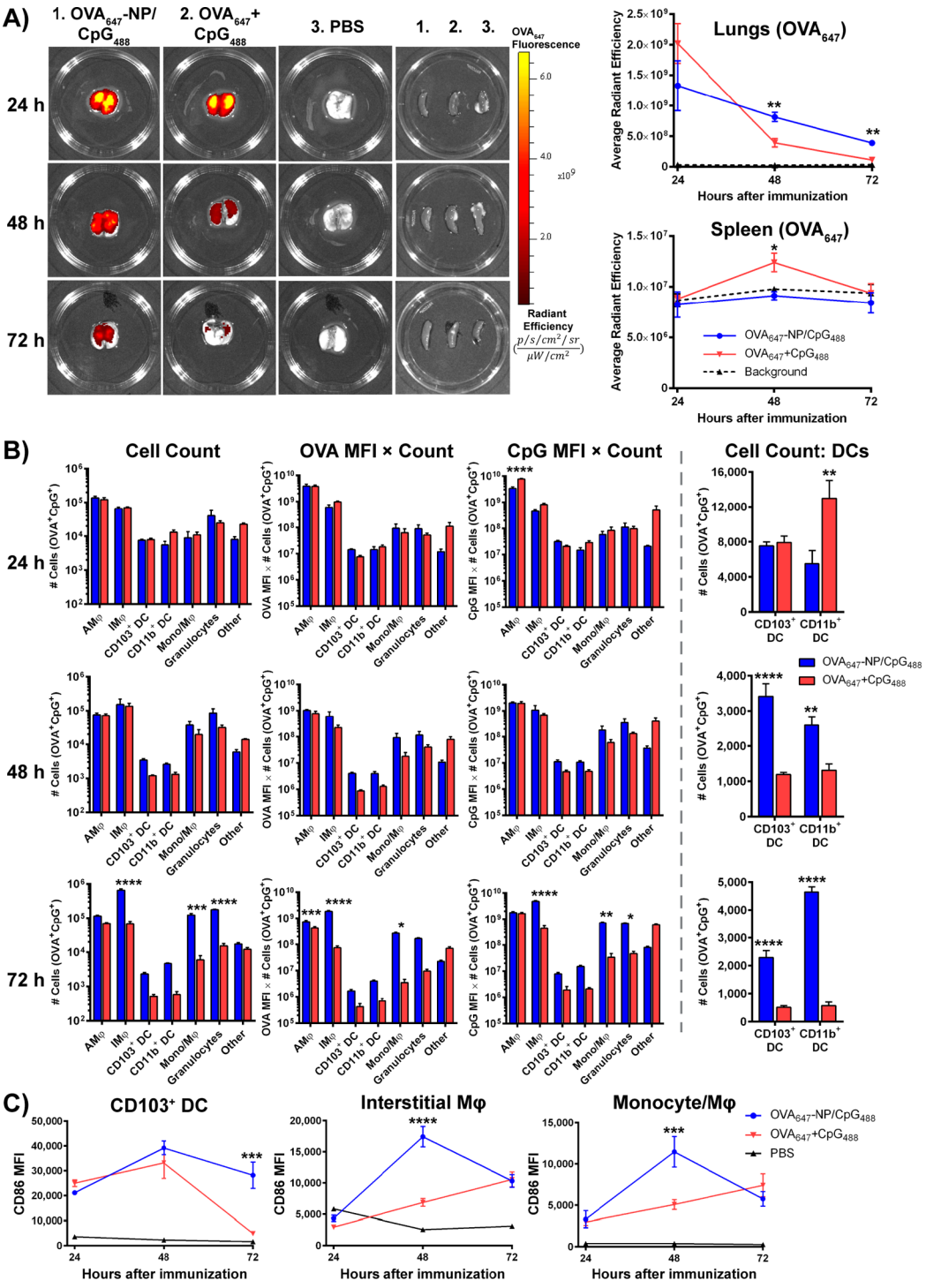

Figure 5. Nanoparticle-mediated dual-delivery enhances colocalization and retention of cargo in pulmonary APCs and expression of activation markers. (A) Lungs and spleens were imaged at 24, 48, and 72 h postimmunization to quantify uptake of OVA_{647}. Representative images of lungs and spleens from each treatment group at each time point (left) and quantification of OVA_{647} fluorescence in lungs and spleens over time (right). (B) Flow cytometry was used to quantify the # of pulmonary APCs positive for both OVA_{647} and CpG_{488} (OVA^+CpG^+) at each time point ("cell count"). Cell counts were also multiplied by either OVA mean fluorescence intensity (MFI) or CpG MFI to determine "relative uptake" of each cargo (MFI × cell count). Bar graphs for $CD103^+$ DC and $CD11b^+$ DC are replicated for visibility. (C) Expression of CD86 was measured for several cell subsets in the lungs. Data are mean ± SEM and representative of four independent experiments, with $n = 3–4$ per group. Immunization dose: 25 μg NP, 7.5 μg OVA, 1.4 μg CpG; *$p < 0.05$, **$p < 0.01$, ***$p < 0.001$, ****$p < 0.0001$ by (A) unpaired t test at each time point comparing OVA–NP/CpG *vs* OVA+CpG, with Holm-Sidak multiple comparisons test, (B) ordinary two-way ANOVA with Sidak's multiple comparisons test, or (C) ordinary two-way ANOVA with Tukey's multiple comparisons test (significance shown for OVA–NP/CpG *vs* OVA+CpG). See also Figure S5.

In addition, CD86 expression was significantly upregulated in certain cell subsets after immunization with OVA–NP/CpG relative to OVA+CpG, including $CD103^+$ DCs, IMφ, and Mono/Mφ (Figure 5C). The increase in expression was

DOI: 10.1021/acsnano.9b00326
ACS Nano 2019, 13, 10939–10960

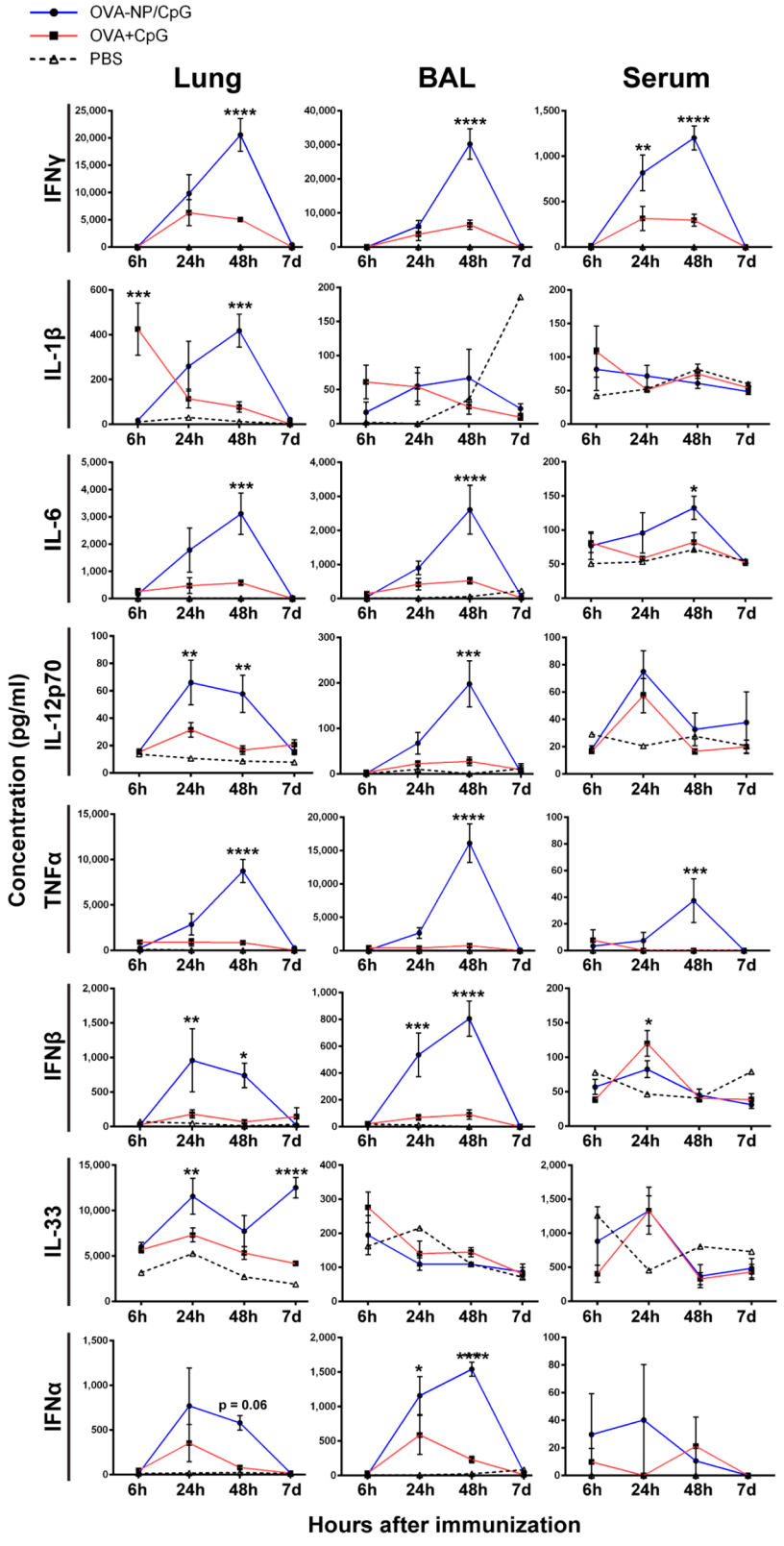

Figure 6. Acute cytokine response to nanoparticle vaccine is localized, transient, and supportive of lung-resident CD8$^+$ T cells. Cytokines associated with CD8$^+$ T cells (IFNγ, IL-1β, IL-6, IL-12p70) and T_{RM} generation (TNFα, IFNβ, IL-33, IFNα) were measured in lungs, BAL, and serum obtained 6 h, 24 h, 48 h, or 7 days after i.n. administration of OVA−NP/CpG or OVA+CpG. Data are mean ± SEM and representative of two independent experiments, with n = 4−5 per group. Immunization dose: 25 μg NP, 7.5 μg OVA, 1.4 μg CpG; *p < 0.05, **p < 0.01, ***p < 0.001, ****p < 0.0001, by ordinary two-way ANOVA with Tukey's multiple comparisons test. Statistical differences shown are for comparison of OVA−NP/CpG *vs* OVA+CpG. See also Figure S6.

DOI: 10.1021/acsnano.9b00326
ACS Nano 2019, 13, 10939−10960

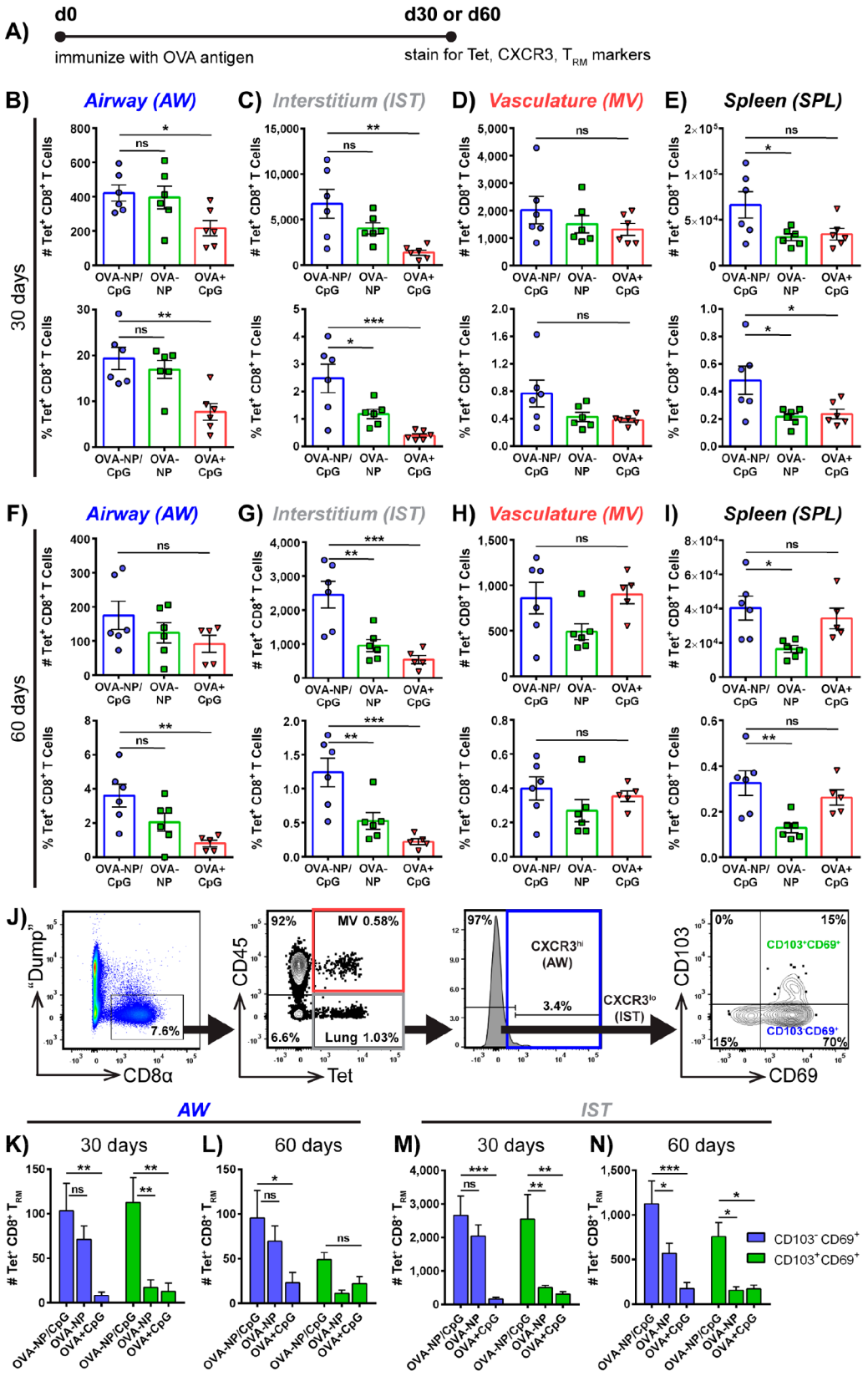

Figure 7. OVA-specific CD8$^+$ T cells are maintained at memory time points and express T_{RM} markers CD69 and CD103. (A) Mice were immunized i.n. with OVA-containing formulations on day 0 and lungs and spleens were analyzed on day 30 or day 60 *via* tetramer and surface marker staining. CXCR3 was used as a marker of AW residence; CD103 and CD69 were used as markers of tissue residency. (B–E) Number (#) and frequency (%) of Tet$^+$ CD8$^+$ T cells in (B) AW, (C) IST, (D) MV, and (E) spleen were enumerated on day 30 after i.n. administration of OVA–NP/CpG, OVA–NP, or OVA+CpG. (F–I) Number (#) and frequency (%) of Tet$^+$ CD8$^+$ T cells in (F) AW, (G) IST, (H) MV, and (I) spleen were enumerated on day 60 after i.n. administration of OVA–NP/CpG, OVA–NP, or OVA+CpG. (J) Flow cytometry was used to quantify Tet$^+$ CD8$^+$ T cells expressing T_{RM} markers (CD103, CD69) in the airway (CXCR3^{hi}) and lung interstitium (CXCR3^{lo}). (K,L) Number

DOI: 10.1021/acsnano.9b00326
ACS Nano 2019, 13, 10939–10960

Figure 7. continued

(#) of Tet$^+$ CD8$^+$ T cells expressing CD69 ± CD103 in AW were enumerated on (K) day 30 or (L) day 60 after immunization. (M,N) Number (#) of Tet$^+$ CD8$^+$ T cells expressing CD69 ± CD103 in IST were enumerated on (M) day 30 or (N) day 60 after immunization. Data are mean ± SEM and representative of two to four independent experiments, with n = 5−6 per group. Immunization dose: 25 μg NP, 7.5 μg OVA, 1.4 μg CpG. Limit of detection: 1 cell (AW), 5 cells (IST/MV), 25 cells (spleen); *p < 0.05, **p < 0.01, ***p < 0.001, ****p < 0.0001, by (B−I) ordinary one-way ANOVA with Tukey's multiple comparisons test or (K−N) ordinary two-way ANOVA with Tukey's multiple comparisons test; ns, not significant. Statistical comparisons are shown for OVA−NP/CpG only.

minimal in AMφ, CD11b$^+$ DCs, and Gran (Figure S5D). This is particularly notable for CD103$^+$ DCs, as this cell subset exhibited lower levels of cargo uptake compared to, for example, Mφ populations, but the subset of CD103$^+$ DCs that did internalize the formulation appears to have been strongly activated, as CD86 expression remained high even after 72 h. Importantly, this cell subset has been implicated in the development of T_{RM} in the lungs.[59] Taken together, these data demonstrate that the NP vaccine enhances persistence and colocalization of vaccine cargo in pulmonary innate immune cells, as well as activation of APCs that can promote a T_{RM} response.

Acute Cytokine Response to Nanoparticle Vaccine Is Localized to the Lungs and Supports Generation of Lung-Resident CD8$^+$ T Cells. The innate immune response generated by a vaccine plays a critical role in shaping the magnitude and phenotype of the resulting adaptive immune response, and this innate response can be characterized in terms of the cytokine profile induced by the vaccine. Evidence suggests that maturation into T_{RM} occurs after activated T cells have migrated back to their home tissue from the lymph nodes, and that the presence of local inflammatory signals in the tissue drives this process.[2,60−62] A number of cytokines are important for generating CD8$^+$ T cell responses (IFNγ, type I interferons (IFNα/β), IL-12, IL-1, IL-6)[63−67] and for the induction and maintenance of T_{RM} (IL-33, IFNα/β, TNFα, IL-12, TGFβ, IL-7, IL-15).[2,54,60,62,68] In particular, several of these cytokines are involved in upregulating T_{RM} surface markers CD69 and CD103; type I IFN, IL-33, and TNFα induce CD69 upregulation on T cells, TGFβ has been shown to induce CD103 expression on T_{RM} precursors, and IL-12 may play a role in differentiation of CD103$^-$CD69$^+$ T_{RM}. Many of these cytokines are also important for rapid activation of pulmonary APC subsets that have been implicated in T_{RM} generation.[69,70]

We hypothesized that the NP vaccine would increase local production of key cytokines in the lungs, leading to an improved pulmonary CD8$^+$ T_{RM} response. To evaluate this, mice were immunized i.n. with OVA−NP/CpG, OVA+CpG, or PBS, and multiplexed cytokine analysis was used to quantify cytokine levels in lung homogenate, BAL, and serum at 6 h, 24 h, 48 h, and 7 days postimmunization. Overall, i.n. administration of the NP vaccine generated 2.5- to 375-fold higher concentrations of cytokines in the lungs and BAL relative to concentrations in the serum, indicating local cytokine production with minimal systemic inflammation (Figure 6). The response peaked at 24 or 48 h before returning to baseline by day 7 postimmunization. The local and acute nature of this cytokine response corroborates histological analyses demonstrating a favorable safety profile for the NP vaccine (Figure S4B). At 24 h and/or 48 h postimmunization, OVA−NP/CpG generated 2- to 10-fold higher levels of cytokines associated with CD8$^+$ T cells (IFNγ, IFNα/β, IL-12p70, IL-1β, IL-6) in the lungs and/or BAL, relative to OVA+CpG. Similarly, concentration of cytokines related to T_{RM} generation (IL-33, TNFα, IFNα/β, IL-12p70) were 2- to 15-fold higher in the lungs and/or BAL at 24 h and/or 48 h after immunization with OVA−NP/CpG, relative to OVA +CpG. We also compared the cytokine response generated by OVA−NP *versus* OVA−NP/CpG. Overall, the OVA−NP formulation generated little to no response above baseline levels, whereas for the majority of cytokines tested, OVA−NP/CpG stimulated significantly higher cytokine concentrations than OVA−NP at the 48 h time point (Figure S6). Thus, CpG appears to be an integral component of stimulating the cytokine response profile observed after immunization with OVA−NP/CpG. Taken together, these data demonstrate that immunization with the NP vaccine generates a local cytokine milieu that supports induction of CD8$^+$ T cells with a T_{RM} phenotype.

Nanoparticle Vaccine Generates Long-Lasting Populations of Lung-Resident Antigen-Specific CD8$^+$ T Cells That Express T_{RM} Surface Markers. The ability of the NP vaccine to enhance the lung-resident CD8$^+$ T cell response after 13 days (Figure 3) prompted us to determine whether antigen-specific CD8$^+$ T cells present in murine lungs at 30 and 60 days after immunization, which are considered memory T cells,[9] possessed a characteristic T_{RM} phenotype. In addition to being defined as CD45$^-$ by i.v. staining, lung T_{RM} have been defined by surface expression of CD69—an activation marker that limits tissue egress by inhibiting expression of sphingosine-1-phosphate receptor—and CD103—an adhesion molecule that binds E-cadherin on epithelial cells and retains T_{RM} in their home tissues.[60] Both CD103$^-$CD69$^+$ and CD103$^+$CD69$^+$ T_{RM} subsets in the lungs have been reported.[15,52] To characterize the memory phenotype of Tet$^+$ CD8$^+$ T cells in the IST and AW, we immunized mice i.n. with a single dose of OVA−NP/CpG, OVA−NP, or OVA+CpG, and on day 30 or day 60 postimmunization, harvested lungs and spleens and quantified Tet$^+$ CD8$^+$ T_{RM}. Here, CXCR3 was used as a marker of airway residence, as previously reported.[21,52,71] Staining with αCD103 and αCD69 antibody was used in conjunction with i.v. αCD45 antibody to identify T_{RM}, and αCXCR3 antibody was used to discriminate AW-resident cells (CXCR3^{hi}) from those resident in the IST (CXCR3^{lo}) (Figure 7A).

At both day 30 (Figure 7B−E) and day 60 (Figure 7F−I) postimmunization, there were significantly more Tet$^+$ CD8$^+$ T cells in the lungs of mice immunized with OVA−NP/CpG relative to those receiving OVA+CpG. There were also generally more cells in the OVA−NP/CpG group relative to mice receiving OVA−NP, although in certain instances, this difference was not statistically significant, consistent with the intrinsic capacity of the NP to enhance the CD8$^+$ T cell response (Figure 3). At day 30, OVA−NP/CpG generated a significantly higher response than OVA+CpG in the AW and IST (Figure 7B,C), but not in the MV or spleen (Figure 7D,E). The number of cells present in the lungs of mice immunized with OVA−NP/CpG were significantly higher in the IST relative to OVA−NP (Figure 7C), but in the AW they were not significantly different (Figure 7B). Although there was no significant difference between any group in the MV (Figure 7D), OVA−NP/CpG generated a

DOI: 10.1021/acsnano.9b00326
ACS Nano 2019, 13, 10939−10960

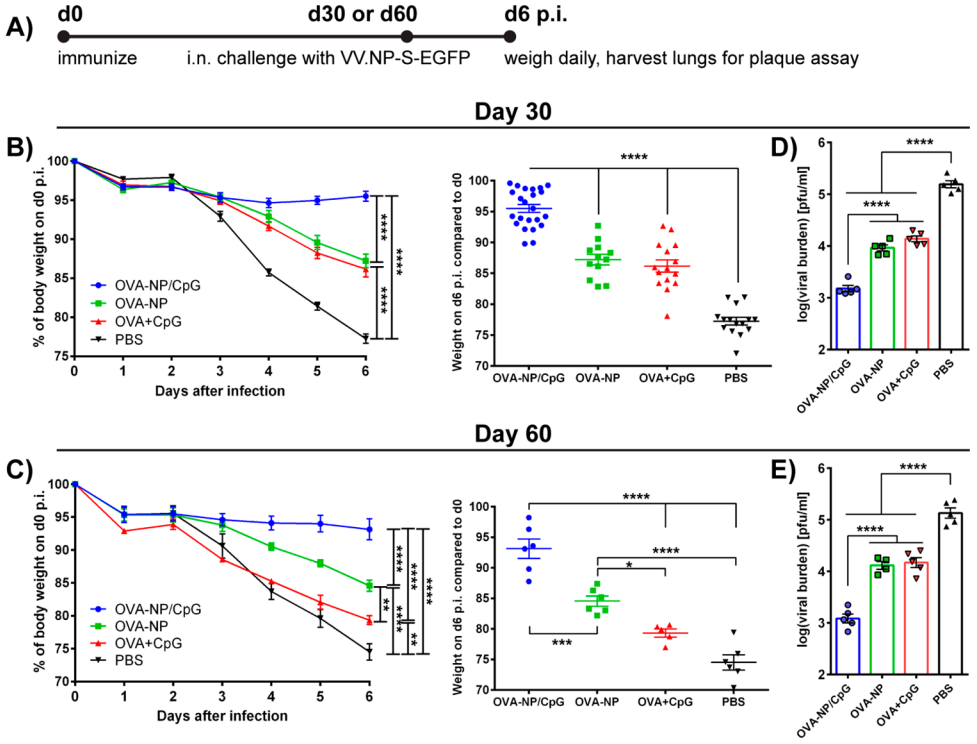

Figure 8. Mice immunized with nanoparticle vaccine exhibit less weight loss and lower viral burden after intranasal challenge with recombinant vaccinia virus. (A) Mice immunized on day 0 were challenged i.n. with recombinant SIINFEKL-expressing vaccinia virus (sublethal dose of 1 × 10^7 pfu/mouse) either 30 or 60 days postimmunization. Mice were weighed daily, and lungs were harvested on day 6 postinoculation (p.i.). (B,C) Percent (%) weight loss in mice challenged on (B) day 30 or (C) day 60 after i.n. administration. Left: weight loss over time. Right: weight at day 6 p.i. expressed as % initial body weight. (D,E) Lungs of mice challenged on (D) day 30 or (E) day 60 postimmunization were harvested on day 6 p.i. for quantification of viral load. Dots show titers for individual animals. Data are mean ± SEM, with (B) n = 12−23 per group, (C) n = 5−6 per group, and (D,E) n = 5 per group. Immunization dose: 25 μg NP, 7.5 μg OVA, 1.4 μg CpG. Data are pooled from one to four independent experiments. Limit of detection for plaque assay = 6 pfu; *p < 0.05, **p < 0.01, ***p < 0.001, ****p < 0.0001, by (B,C, left) repeated measures two-way ANOVA with Tukey's multiple comparisons test or (B,C, right; D,E) ordinary one-way ANOVA with Tukey's multiple comparisons test.

significantly higher response than OVA−NP in the spleen (Figure 7E). At day 60, there were significantly more cells in the IST for the OVA−NP/CpG group relative to both OVA−NP and OVA+CpG (Figure 7G), whereas the difference between groups in the AW was less pronounced (Figure 7F). Again, there was no significant difference between any group in the MV (Figure 7H), whereas OVA−NP/CpG continued to produce a significantly higher response in the spleen relative to OVA−NP (Figure 7I). Although in most cases the OVA−NP formulation produced a greater response than OVA+CpG, at day 60, it remained inferior to OVA−NP/CpG in the IST, where the majority of $CD8^+$ T_{RM} are located. Overall, these data show that the NP vaccine is able to enhance generation of lung-resident $CD8^+$ T cells that are maintained for at least 60 days after immunization.

We next asked whether long-lasting antigen-specific $CD8^+$ T cells in the lungs expressed characteristic T_{RM} surface markers. At these same time points, AW ($CXCR3^{hi}$) and IST ($CXCR3^{lo}$) cells were analyzed for CD103 and CD69 expression (Figure 7J). At day 30, i.n. administration of OVA−NP/CpG elicited significantly more AW and IST Tet^+ $CD8^+$ T_{RM} with both $CD103^-CD69^+$ and $CD103^+CD69^+$ phenotypes when compared to immunization with OVA+CpG (Figure 7K,M). There were also significantly more AW and IST $CD8^+$ T_{RM} of the $CD103^+CD69^+$ phenotype in the OVA−NP/CpG group relative to the OVA−NP group (green bars); for the $CD103^-CD69^+$ phenotype (blue bars), this difference was not significant, although the number of cells was still higher. At day 60, in the IST, OVA−NP/CpG induced significantly more $CD8^+$ T_{RM} of both phenotypes than either control group (OVA−NP and OVA+CpG) (Figure 7N). In the AW, this difference was only significant for OVA−NP/CpG *versus* OVA +CpG in the $CD103^-CD69^+$ phenotype, although OVA−NP/CpG still produced the highest number of cells of both phenotypes (Figure 7L). These data indicate that the NP vaccine is superior to control formulations for generating antigen-specific $CD8^+$ T_{RM} in the lungs, particularly at 60 days after immunization.

Single-Dose Pulmonary Immunization with Nanoparticle Vaccine Protects Against Sublethal Respiratory Virus Challenge. Ultimately, an effective vaccine must generate T cells that protect against subsequent infectious challenge. Given the ability of a single i.n. dose of the NP vaccine to generate antigen-specific $CD8^+$ T_{RM} and retain them in the lungs for up to 60 days postimmunization, we next determined whether these T_{RM} were protective against infection with a respiratory virus. To do this, we immunized mice i.n. with OVA−NP/CpG, OVA−NP, OVA+CpG, or PBS. On day 30 or day 60 postimmunization, mice were challenged i.n. with a recombinant vaccinia virus expressing influenza virus nucleoprotein, SIINFEKL peptide, and enhanced green fluorescent protein (VV.NP-S-EGFP). As this virus expresses the SIINFEKL epitope of OVA, it provides a tool for evaluating the ability of NP vaccine-induced $CD8^+$ T cells to protect against

DOI: 10.1021/acsnano.9b00326
ACS Nano 2019, 13, 10939−10960

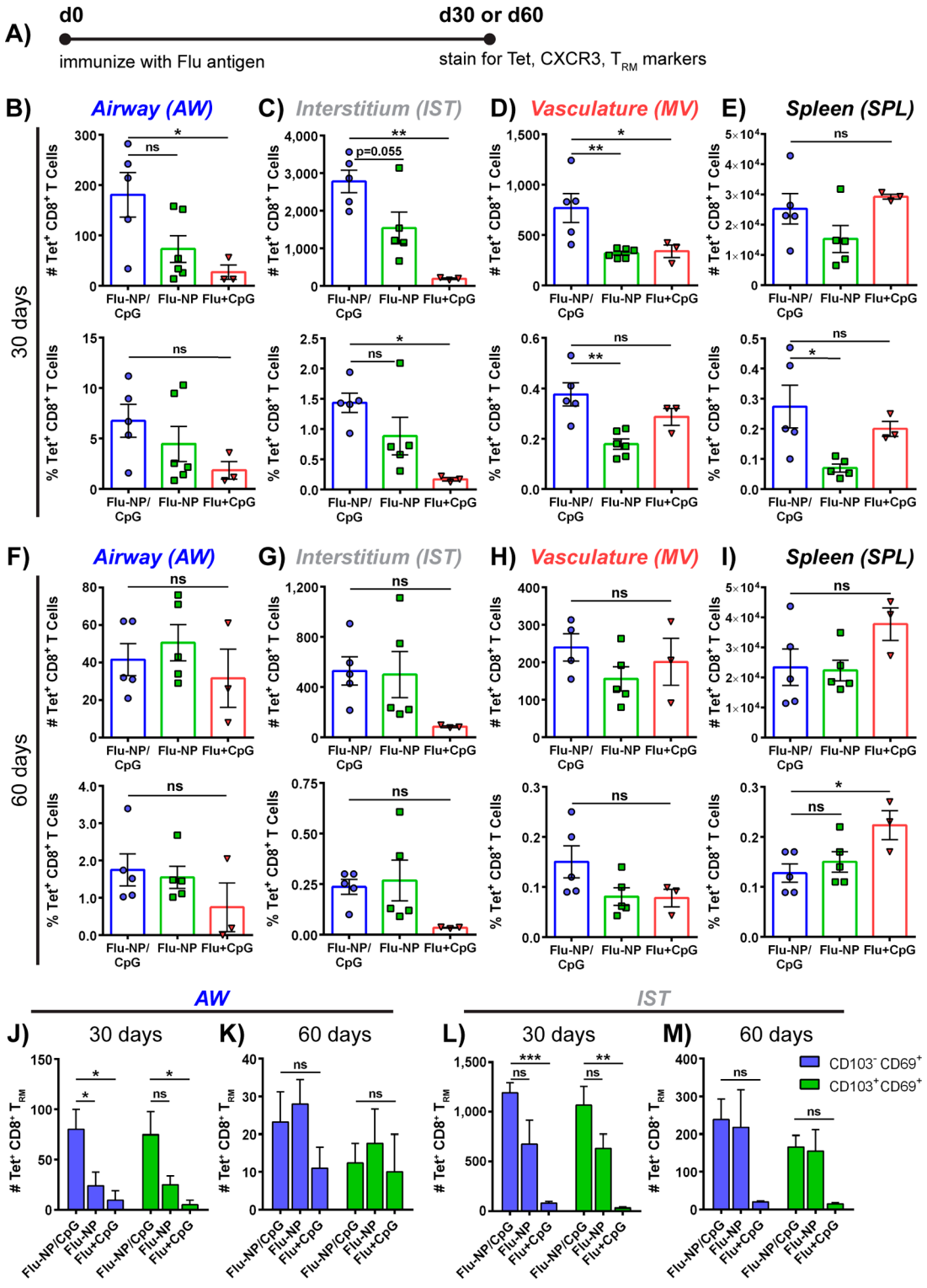

Figure 9. Flu-specific CD8⁺ T cells are maintained at memory time points and express T_{RM} markers CD69 and CD103. (A) Mice were immunized i.n. with Flu-containing formulations on day 0 and lungs and spleens were analyzed on day 30 or day 60 *via* Tet and surface marker staining. CXCR3 was used as a marker of AW residence; CD103 and CD69 were used as markers of tissue residency. (B–E) Number (#) and frequency (%) of Tet⁺ CD8⁺ T cells in (B) AW, (C) IST, (D) MV, and (E) spleen were enumerated on day 30 after i.n. administration of Flu–NP/CpG, Flu–NP, or Flu+CpG. (F–I) Number (#) and frequency (%) of Tet⁺ CD8⁺ T cells in (F) AW, (G) IST, (H) MV, and (I) spleen were enumerated on day 60 after i.n. administration of Flu–NP/CpG, Flu–NP, or Flu+CpG. (J–M) Number (#) of Tet⁺ CD8⁺ T cells expressing CD69 ± CD103 in AW were enumerated on (J) day 30 or (K) day 60 after immunization. (L–M) Number (#) of Tet⁺ CD8⁺ T cells expressing CD69 ± CD103 in IST were enumerated on (L) day 30 or (M) day 60 after immunization. Data are mean ± SEM, with $n = 3–6$ per group, and representative of two independent experiments. Immunization dose: 25 μg NP, 9.5 μg Flu, 1.4 μg CpG. Limit of detection: 1 cell (AW), 5 cells (IST/MV), 25 cells (spleen); *$p < 0.05$, **$p < 0.01$, ***$p < 0.001$, by (B–I) ordinary one-way ANOVA with Tukey's multiple comparisons test or (J–M) ordinary two-way ANOVA with Tukey's multiple comparisons test; ns, not significant.

DOI: 10.1021/acsnano.9b00326
ACS Nano 2019, 13, 10939–10960

i.n. challenge. Mice were inoculated with a sublethal dose (1×10^7 pfu) of the virus and weighed daily through day 6 postinoculation (p.i.) (Figure 8A). On day 6 p.i., lungs were harvested for quantification of viral load.

At both day 30 and day 60, mice immunized with the NP vaccine were significantly protected from challenge-induced weight loss relative to all other formulations. Mice immunized with OVA−NP/CpG lost ∼5−7% of body weight by day 6 p.i. *versus* a loss of ∼13−26% in other groups (Figure 8B,C). Additionally, the OVA−NP/CpG group in the 30 day cohort began regaining weight by day 5 p.i. (Figure 8B).

To further validate these findings, viral load was quantified in lungs harvested from infected mice at day 6 p.i. There was a 1−2 log reduction in viral burden in the lungs of mice immunized with OVA−NP/CpG, relative to the other formulations, at both day 30 and day 60 postimmunization (Figure 8D,E). Overall, these results demonstrate that a single dose of the NP vaccine provides significant $CD8^+$ T_{RM}-mediated protection against respiratory virus challenge in an antigen-specific manner.

Nanoparticle Vaccine Containing Influenza Virus Protein Generates Antigen-Specific $CD8^+$ T_{RM} in the Lungs. After demonstrating the ability of the NP vaccine to generate $CD8^+$ T_{RM} in the lungs and protect against respiratory virus challenge using a model antigen (OVA), we next asked whether these findings could be applied to a more clinically relevant antigen and infection model. To this end, we shifted our focus to influenza, a respiratory infection of global importance and a significant public health challenge.[72] It is well-established that $CD8^+$ T_{RM} cells are important for generating heterosubtypic immunity against influenza A viruses in both mice and humans.[15,18,24,55] To evaluate the ability of the NP vaccine to protect against this pathogen, we selected nucleoprotein, a structural protein from influenza A H1N1 virus (strain A/Puerto Rico/8/1934; PR8), as the antigen, as there is precedent for using the PR8 strain in murine influenza challenge models. Whereas surface proteins like hemagglutinin and neuraminidase are commonly used in experimental flu vaccines to generate a humoral response, internal viral antigens like nucleoprotein are known to contain the majority of influenza $CD8^+$ T cell epitopes.[73−75] Thus, using nucleoprotein as a vaccine antigen lends itself to specifically studying the protective effect of an immunization-induced $CD8^+$ T cell response. In addition, because $CD8^+$ T cell epitopes of influenza A virus are largely conserved across strains and subtypes, they may be particularly well-suited for providing broad protection, and although $CD8^+$ T cells typically do not generate sterilizing immunity, they are useful for reducing disease severity and pathogen transmission.[24,73,76,77]

We will henceforth refer to the nucleoprotein antigen as "Flu" to avoid confusion with the "NP" abbreviation for nanoparticle. Thus, formulations will be indicated as Flu−NP/CpG (nucleoprotein conjugated to nanoparticle and complexed with CpG), Flu−NP (nucleoprotein conjugated to nanoparticle), and Flu+CpG (soluble nucleoprotein mixed with CpG). We first validated that the Flu antigen could be covalently conjugated to NP *via* the same chemistry used to load OVA protein. Flu protein was thiolated as described for OVA and reacted with pH-responsive NP to generate Flu−NP conjugates (Figure S7A). Flu−NP conjugates were then electrostatically complexed with CpG to create Flu−NP/CpG (Figure S7B). Both Flu−NP/CpG and Flu−NP were characterized by dynamic light scattering (DLS) (Figure S7C).

We next assessed the ability of Flu−NP/CpG and related control formulations to generate antigen-specific $CD8^+$ T cells expressing lung T_{RM} markers at memory time points ($CD103^-CD69^+$ and $CD103^+CD69^+$ $CD8^+$ T_{RM}). To do this, we prepared a fluorescent MHC-I tetramer containing ASNENMETM peptide, a known immunodominant H-$2D^b$ epitope for nucleoprotein from PR8 virus.[78] We then immunized mice i.n. with a single dose of Flu−NP/CpG, Flu−NP, or Flu+CpG, and on day 30 or day 60 postimmunization, harvested lungs and spleens, and quantified Tet^+ $CD8^+$ T cells in the same manner as described for OVA (Figure 9A). Similarly, we also assessed expression of T_{RM} markers CD69 and CD103 on the antigen-specific $CD8^+$ T cell populations in the AW and IST lung compartments.

At day 30, mice immunized with Flu−NP/CpG had significantly more Tet^+ $CD8^+$ T cells in the AW, IST, and MV compartments than mice immunized with Flu+CpG (Figure 9B−D). The difference between Flu−NP/CpG and Flu−NP groups was less pronounced, with significance only in the MV; however, a general trend of greater numbers of Tet^+ $CD8^+$ T cells produced by Flu−NP/CpG in the lungs was observed. There was no significant difference between treatment groups in the spleen (Figure 9E). At day 60, the number of cells generated by the Flu−NP/CpG, Flu−NP, and Flu+CpG groups was not significantly different in any lung compartment or in the spleen (Figure 9F−I), though in the IST, both Flu−NP/CpG and Flu−NP exhibited cell counts higher than those of Flu+CpG (Figure 9G). These data show that, similarly to the NP vaccine containing OVA, the NP vaccine with Flu antigen is able to generate higher numbers of lung-resident $CD8^+$ T cells that are maintained for at least 30 days after immunization. However, by 60 days, they have waned to similar levels as those seen in control groups.

We next examined whether these long-lasting antigen-specific $CD8^+$ T cells in the lungs expressed T_{RM} surface markers. At 30 and 60 days postimmunization, AW ($CXCR3^{hi}$) and IST ($CXCR3^{lo}$) cells were analyzed for CD103 and CD69 expression, as previously shown in Figure 7J. At day 30, Flu−NP/CpG immunization generated more T_{RM} of both phenotypes ($CD103^-CD69^+$ and $CD103^+CD69^+$) in both the AW and IST (Figure 9J,L). Again, at day 60, the differences between treatment groups were less pronounced, with the Flu−NP group in some instances producing equivalent or greater numbers of T_{RM} relative to the Flu−NP/CpG (Figure 9K,M). Both Flu−NP/CpG and Flu−NP were superior to Flu+CpG in the IST (Figure 9L,M). Overall, these data indicate that immunization with a nanoparticle-containing formulation is superior to a soluble formulation for generating Flu-specific $CD8^+$ T_{RM} in the lungs, and that addition of CpG adjuvant increases efficacy similarly to what was observed with model antigen (OVA).

Single-Dose Pulmonary Immunization with Nanoparticle Vaccine Protects Against Lethal Challenge with Influenza A H1N1 Virus. As with previous experiments using OVA protein antigen, the ultimate test of efficacy for a vaccine is its ability to protect against infection. Thus, we sought to determine whether a single dose of NP vaccine with Flu antigen could similarly protect against respiratory challenge. To this end, we immunized mice i.n. with Flu−NP/CpG, Flu−NP, Flu+CpG, or PBS, and on day 30 or day 60 postimmunization, challenged i.n. with PR8 virus. In this lethal challenge model, mice were inoculated with 200 FFU of PR8, a dose at which untreated animals experience severe weight loss and disease

DOI: 10.1021/acsnano.9b00326
ACS Nano 2019, 13, 10939−10960

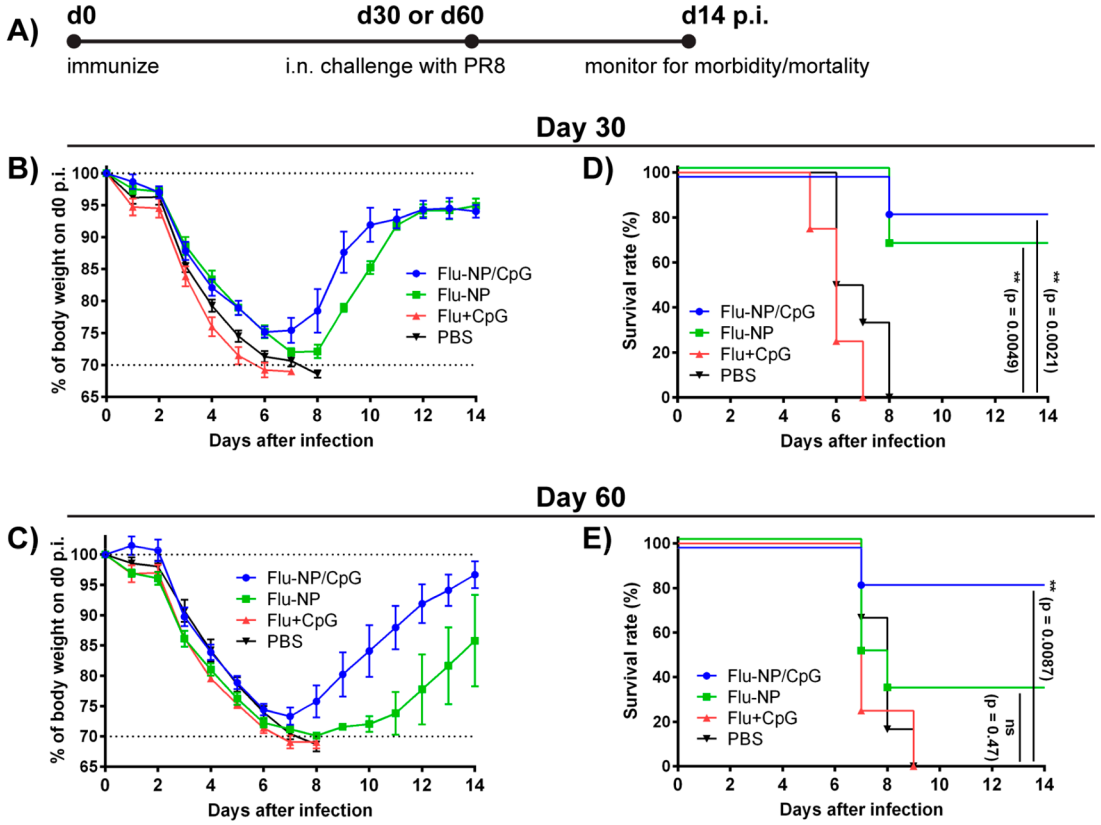

Figure 10. Mice immunized with nanoparticle vaccine exhibit improved survival after intranasal challenge with influenza A H1N1 virus. (A) Mice immunized on day 0 were challenged i.n. with influenza A H1N1 PR8 virus (lethal dose of 200 FFU/mouse) either 30 or 60 days postimmunization. Mice were weighed daily and evaluated for morbidity/mortality. (B,C) Percent (%) weight loss in mice challenged on (B) day 30 or (C) day 60 after i.n. administration. (D,E) Survival of mice challenged on (D) day 30 or (E) day 60 postimmunization. Mice that exceeded 30% weight loss were considered deceased. Data are mean ± SEM, with n = 4−6 per group, from two independent experiments. Immunization dose: 25 μg NP, 9.5 μg Flu, 1.4 μg CpG. Statistical significance in survival curves was determined with a Mantel−Cox log-rank test (p < 0.01; ns, not significant).**

symptoms. Mice were monitored daily through day 14 p.i. for weight loss, morbidity, and mortality (Figure 10A).

At day 30, mice immunized with either Flu−NP/CpG or Flu−NP were protected from challenge-induced weight loss relative to Flu+CpG and naïve (PBS-treated) mice (Figure 10B). Mice in the Flu−NP/CpG and Flu−NP groups lost less weight overall and, around day 7 p.i., began to recover instead of continuing to lose weight. In addition, 83% of Flu−NP/CpG mice and 67% of Flu−NP mice survived challenge, whereas 100% of Flu+CpG mice and PBS mice succumbed to infection (>30% weight loss) by day 7 or day 8 p.i., respectively (Figure 10D).

At day 60, the protective effect of the Flu−NP/CpG formulation was maintained (Figure 10C), consistent with results seen in the vaccinia challenge model. In addition, the survival rate for the Flu−NP/CpG group was the same (83%), whereas for the Flu−NP group it dropped to 33% (Figure 10E). As before, 100% of mice in the Flu+CpG and PBS groups perished by day 9 p.i. Overall, these results demonstrate that a single dose of the NP vaccine formulated with a clinically relevant antigen (influenza A nucleoprotein) offers protection against lethal respiratory virus challenge. Nucleoprotein is an internal viral protein, and so it is a target for protective T cell responses. Given that T_{RM} specific for the immunodominant $CD8^+$ T cell epitope of nucleoprotein are detected at the highest frequency in lungs of mice immunized with Flu−NP/CpG, our data suggest these $CD8^+$ T_{RM} cells contribute to protection.

CONCLUSION

As the importance of tissue-resident memory T cells in defense against disease becomes increasingly clear, efforts are turning toward developing mucosal vaccines that can induce a strong and protective T_{RM} response against infectious pathogens and cancers.[13,26,43,44,79−82] Here, using a mouse model of pulmonary immunization, we demonstrated that a single dose of pH-responsive NP vaccine provided extended co-delivery of antigen and adjuvant to pulmonary APCs, produced a cytokine milieu supportive of tissue-resident $CD8^+$ cells, induced a $CD8^+$ T_{RM} response that persisted for up to 60 days after immunization, and was protective against both lethal and sublethal challenge with respiratory viruses (influenza and vaccinia, respectively). Antigen-specific $CD8^+$ T cells displayed surface markers characteristic of T_{RM} (CD103, CD69), and intravascular staining showed them to be resident in the lung interstitium ($CD45^-CXCR3^{lo}$) and airways ($CD45^-CXCR3^{hi}$). Both the pH-responsive functionality of the carrier and its capacity for dual-delivery were crucial for inducing a $CD8^+$ T_{RM} response, which highlights the significance of engineering nanomaterial properties in the design of T_{RM} vaccines. We also showed that the route of administration was important for generating lung-resident cells; i.n. administration of the NP vaccine induced more antigen-specific $CD8^+$ T cells in the IST and AW than did s.c. immunization. Notably, unlike previous reports of T_{RM} vaccines in which multiple doses were administered, these

DOI: 10.1021/acsnano.9b00326
ACS Nano 2019, 13, 10939−10960

results were obtained with a single dose, which offers potential translational advantages such as increased compliance and dose reduction.

Our findings suggest that several key properties of the NP vaccine are linked to the resulting $CD8^+$ T_{RM} response. It has been proposed that local antigen recognition and persistence in nonlymphoid tissues, including the lungs, can promote formation of T_{RM} cell populations.[47,54,83,84] Takamura *et al.* found that $CD8^+$ T cell encounter with cognate antigen in the lung, but not in the lung-draining lymph node, was critical to conversion from circulating to resident cells in the lungs.[20] Notably, the NP we describe here increased retention of vaccine cargo in pulmonary APCs for up to 3 days after pulmonary immunization. This finding suggests that NP-mediated delivery can extend antigen residence in the lungs over soluble antigen formulations and enhance the pulmonary $CD8^+$ T_{RM} response. This could be due to the cationic surface charge of the NP, which may confer mucoadhesive properties that extend residence time in the lungs.[69,85] It could also reflect the capacity of pH-responsive NP carriers to prolong intracellular residence time by avoiding endosomal recycling and lysosomal degradation.[41] Longer-term studies that further examine the duration of antigen persistence and its effects on the T_{RM} response are warranted and may motivate the use of pH-responsive materials as particle depots to control antigen release and delivery.

It has also been reported that certain pulmonary APC subsets, including $CD103^+$ DCs and alveolar macrophages, can promote establishment of lung T_{RM}.[55−57] In our experiments, alveolar macrophages took up large amounts of OVA and CpG over the course of 72 h and therefore may have contributed to the T_{RM} response. More importantly, we observed uptake in $CD103^+$ dendritic cells, the predominant cross-presenting DC subset in mucosal tissues.[86,87] The pH-responsive nature of the NP, which allows it to transport antigen to the cytosol, potentially facilitates cross-presentation and priming of $CD8^+$ T_{RM} responses by $CD103^+$ DCs. The relative contributions that NP-mediated cytosolic antigen delivery *versus* intrinsic mechanisms of DC cross-presentation provide in the induction of a $CD8^+$ T_{RM} response in the lungs merit further investigation. We speculate that both mechanisms contribute to the response. In addition, we found that $CD103^+$ DCs were the cell type most potently activated by the NP vaccine, with CD86 expression sustained for at least 3 days postimmunization. NP delivery enhanced colocalization of CpG with OVA in $CD103^+$ DCs during this time, which likely contributed to robust CD86 expression.[88] Methods of guiding vaccine delivery specifically to $CD103^+$ DCs (*e.g.*, antibody targeting) may be a promising approach for increasing vaccine uptake in this APC subset that is important for promoting T_{RM} formation.[55]

Several surface markers have been used to describe T_{RM} cells in various nonlymphoid tissues—in particular, CD103 and CD69.[18,80,89] However, these markers are not found on all T_{RM}; many T_{RM} populations located outside epithelia do not express CD103.[90] CD69 is more universally expressed and has been suggested to influence accumulation and retention of $CD8^+$ T cells in the lungs during the early stages of infection.[20] Both $CD103^-CD69^+$ and $CD103^+CD69^+$ T_{RM} subsets have been shown in the lungs.[52,91,92] In our experiments, we found the $CD103^-CD69^+$ phenotype to be somewhat more prevalent than $CD103^+CD69^+$ in the IST and AW. It has been suggested that infiltration of tumors with $CD8^+$ T_{RM} expressing CD103 correlates to longer survival of patients with a variety of cancers, including breast, lung, ovarian, cervical, and bladder.[60] Notably, TGFβ is needed to induce expression of CD103 on T_{RM},[62,93,94] and we were unable to detect this cytokine at several time points after immunization. In light of this, methods to tailor the NP vaccine to stimulate TGFβ production or otherwise generate more CD103-expressing $CD8^+$ T_{RM} cells may warrant further study. Nevertheless, the NP vaccine provided significant protection against challenge with multiple respiratory viruses, demonstrating its translational promise.

In conclusion, this report demonstrates generation of protective $CD8^+$ T_{RM} in the lungs with a single mucosally administered dose of a pH-responsive nanoparticle vaccine. Intranasal dual-delivery of antigen and adjuvant with pH-responsive NP was shown to enhance the magnitude and functionality of the lung-resident $CD8^+$ T cell response, as well as increase antigen persistence and activation in pulmonary APCs. Efficacy of the nanoparticle vaccine was demonstrated with both a model antigen (ovalbumin) and a clinically relevant antigen (influenza A nucleoprotein). Antigen-specific $CD8^+$ T cells in the lungs displayed characteristic T_{RM} markers at memory time points, and mice were protected against respiratory virus infection in both sublethal and lethal challenge models. The use of intravascular staining to identify lung-resident cells, in conjunction with staining for markers of tissue resident memory, has enabled relationships between NP vaccine properties and the generation of T_{RM} to be established. This NP vaccine provides a modular platform technology for delivery of any number of clinically relevant protein or peptide antigens, as well as other nucleic acid adjuvants. Additionally, there are several practical advantages to this system that lend themselves to the possibility of scale-up and translation, such as the ability to synthesize NP on a large scale and sterilize them by filtration.[95] It would also be feasible to develop this vaccine as a needle-free aerosol formulation, to facilitate clinical translation and simple administration without the need for skilled healthcare workers. Overall, this NP system represents a promising technology for the development of T_{RM} vaccines against respiratory infections such as influenza, other pathogens that target nonlymphoid tissues, and mucosal cancers.

METHODS

RAFT Synthesis of (PDSMA-*co*-DMAEMA)-*b*-(PAA-*co*-BMA-*co*-DMAEMA). RAFT copolymerization of pyridyl disulfide ethyl methacrylate (PDSMA) and dimethylaminoethyl methacrylate (DMAEMA) was conducted under a nitrogen atmosphere in dioxane (40 wt % monomer) at 30 °C for 18 h, as previously described.[37] PDSMA monomer was synthesized according to a previously reported procedure.[96] The RAFT chain transfer agent (CTA) used was 4-cyano-4-(ethylsulfanylthiocarbonyl) sulfanylpentanoic acid (ECT) and the initiator used was 2,2′-azobis(4-methoxy-2,4-dimethylvaleronitrile) (V-70) (Wako Chemicals, Richmond, VA). The initial molar ratio of DMAEMA to PDSMA was 92:8, and the initial monomer ($[M]_0$) to CTA ($[CTA]_0$) to initiator ($[I]_0$) ratio was 100:1:0.05. The resultant poly(PDSMA-*co*-DMAEMA) macro-chain transfer agent (mCTA) was isolated by precipitation (6×) into pentane. A schematic of the mCTA polymerization reaction can be found in Scheme S1A.

Purified mCTA was dried *in vacuo* for 1 week and used for block copolymerization with DMAEMA, propylacrylic acid (PAA), and butyl methacrylate (BMA) to create a pH-responsive polymer, as described previously.[37,97] DMAEMA (30%), PAA (30%), and BMA (40%) ($[M]_0/[mCTA]_0$ = 450) were added to the mCTA dissolved in dimethylacetamide (DMAc) (40 wt % monomer and mCTA) along with V-70 initiator ($[mCTA]_0/[I]_0$ = 2.5). Polymerization took place under a nitrogen atmosphere for 24 h at 30 °C. The resultant diblock copolymer was isolated by dialysis against acetone using a 3.5 kDa MWCO membrane, followed by dialysis against deionized water. The

DOI: 10.1021/acsnano.9b00326
ACS Nano 2019, 13, 10939−10960

purified diblock copolymer was lyophilized for 72 h prior to use. A schematic of the pH-responsive polymerization reaction can be found in Scheme S1B.

Polymer composition and monomer conversion of both the mCTA and diblock copolymer were characterized by ^{1}H NMR spectroscopy ($CDCl_3$) on a Bruker AV400 spectrometer (Figure S1A,B). Gel permeation chromatography (GPC, Agilent) with DMF containing 0.1 M LiBr as the mobile phase and in-line light scattering (Wyatt) and refractive index (Agilent) detectors was used to determine molecular weight (MW) and polydispersity indices (PDI) of both the mCTA and diblock copolymer (Figure S1D and Table S1). Molecular weights were determined using dn/dc values calculated previously (0.071 for mCTA and 0.065 for diblock). Characterization was done according to previously published methods.[37] Representative NMR spectra, GPC traces, and a summary of polymer properties can be found in Figure S1 and Table S1.

RAFT Synthesis of (PDSMA-*co*-DMAEMA)-*b*-(BMA). Purified mCTA used for the synthesis described above was also used for block copolymerization with poly(butyl methacrylate) (pBMA) to create a non-pH-responsive control polymer. Monomer was added to mCTA ($[M]_0/[mCTA]_0 = 300$) and dissolved in dioxane (40 wt % monomer and mCTA) along with V-70 initiator ($[mCTA]_0/[I]_0 = 20$), then polymerized under a nitrogen atmosphere for 24 h at 35 °C. The resultant diblock copolymer was isolated by dialysis as described above. The purified polymer was then lyophilized, and its composition, molecular weight, and polydispersity index were analyzed using ^{1}H NMR ($CDCl_3$) spectroscopy and GPC (Figure S1C,D and Table S1), according to previously published methods.[98] The control polymerization reaction can be seen in Scheme S1C.

Preparation and Characterization of Nanoparticles. Self-assembled micellar nanoparticles were obtained by first dissolving lyophilized polymer at 50 mg/mL in 100% ethanol, then rapidly pipetting dissolved polymer into 100 mM phosphate buffer (pH 7) to a final concentration of 10 mg/mL. Nanoparticles were formulated in the same way for both pH-responsive (NP_{pH}) and control (NP_{ctrl}) polymers. For *in vivo* studies, ethanol was removed by buffer exchange into PBS (pH 7.4) *via* three cycles of centrifugal dialysis (Amicon, 3 kDa MWCO, Millipore), and NP solutions were then sterilized *via* syringe filtration (Whatman, 0.22 μm, GE Healthcare). Final polymer concentration was determined with UV−vis spectrometry (Synergy H1Multi-Mode Reader, BioTek) by measuring absorbance of aromatic PDS groups at 280 nm. The size of the NP was measured *via* DLS. NP solutions were prepared at a concentration of 0.1−0.2 mg/mL in PBS (pH 7.4), and the hydrodynamic radius was measured using a Malvern Instruments Zetasizer Nano ZS Instrument (Malvern, USA). Representative DLS data for both polymers at physiological pH (7.4) can be found in Figure S1E. In addition, size change of NP_{pH} but not NP_{ctrl} at pH 5.8, as measured by DLS, can be seen in Figure S1F (left).

Erythrocyte Lysis Assay. The degree to which the pH-responsive polymer was able to induce pH-dependent lysis of lipid bilayer membranes (thus leading to cytosolic delivery) was assessed *via* a red blood cell hemolysis assay as previously described.[99] Briefly, polymers (10 μg/mL) were incubated for 1 h at 37 °C in the presence of human erythrocytes in 100 mM sodium phosphate buffer. Buffers in the pH range of the endosomal processing pathway (7.4, 7.0, 6.6, 6.2, and 5.8) were used. Extent of cell lysis (*i.e.*, endosomolytic activity) was determined *via* UV−vis spectrometry by measuring the amount of hemoglobin released (Abs = 541 nm) (Figure S1F, right). Absorbances were normalized to a 100% lysis control (1% Triton X-100). Samples were run in quadruplicate.

Preparation of Antigen−Nanoparticle Conjugates. A model antigen, ovalbumin protein (OVA), was conjugated to pendant PDS groups on NP *via* thiol−disulfide exchange. For conjugate characterization, OVA from chicken egg white (MilliporeSigma) was used; for *in vivo* studies, endotoxin-free (<1 EU/mg) EndoFit OVA (Invivogen) was used. In some experiments, OVA was labeled with fluorescein isothiocyanate isomer (FITC; Sigma) for evaluating conjugation efficiency *via* fluorescent imaging of SDS-PAGE gels, or with Alexa Fluor 647-NHS ester (AF647; Thermo Fisher Scientific) for tracking conjugates after *in vivo* administration. Following manufacturer's instructions, dye was added to OVA for a degree of labeling of ∼1 FITC/OVA or ∼0.5 AF647/OVA.

To prepare OVA for conjugation, free amines on the protein were thiolated by incubation with ∼25 molar excess of 2-iminothiolane (Traut's Reagent, Thermo Fisher Scientific) in reaction buffer (100 mM phosphate buffer, pH 8, supplemented with 1 mM EDTA) as previously described.[37] Unreacted 2-iminothiolane was removed by buffer exchanging thiolated OVA into 1× PBS (pH 7.4) using Zeba Spin desalting columns (0.5 mL, 7 kDa MWCO, Thermo Fisher Scientific). For *in vivo* studies, thiolated OVA was sterilized *via* syringe filtration (0.22 μm, Millipore). Following manufacturer's instructions, the molar ratio of thiol groups to OVA protein was determined with Ellman's reagent (Thermo Fisher Scientific) to be ∼3−5 thiols/OVA. Polymer NP solutions were reacted with thiolated OVA at various molar ratios of pH-responsive NP:OVA (5:1, 10:1, 20:1) or control NP:OVA (3.5:1, 7:1, 14:1) to make OVA−NP_{pH} and OVA−NP_{ctrl} conjugates, respectively. The conjugation ratio for the control polymer was adjusted to maintain a constant dose of antigen for both carriers. Conjugation was done overnight, in the dark, at room temperature, and under sterile conditions (when needed), as previously described.[37] Antigen conjugation was verified *via* nonreducing SDS-polyacrylamide gel electrophoresis (SDS-PAGE) using 4−20% Mini-Protean TGX Precast protein gels (Bio-Rad) (Figure S2A). Gels were run at 130 V for 1 h and imaged with a Gel Doc EZ System (Bio-Rad). A conjugation ratio of 5:1 (pH) or 3.5:1 (ctrl) was used for all *in vivo* formulations in order to maximize the amount of antigen delivered. DLS was used to measure the size of OVA−NP conjugates, as described above (Figure S2C, top and bottom left).

Influenza A H1N1 nucleoprotein (Flu) formulated in sterile phosphate buffer was obtained from Sino Biological (Beijing, China). To prepare Flu antigen for conjugation, free amines were thiolated by incubation with ∼250 molar excess of 2-iminothiolane in reaction buffer. Unreacted 2-iminothiolane was removed by buffer exchange into sterile 1× PBS. Following the manufacturer's instructions, the molar ratio of thiol groups to Flu protein was determined with a Measure-iT thiol assay kit (Thermo Fisher Scientific). The concentration of Flu protein after thiolation and purification was measured using the Pierce Rapid Gold BCA protein assay kit (Thermo Fisher Scientific). In some cases, Flu was labeled with AF647 prior to thiolation for evaluating conjugation efficiency *via* fluorescent imaging of SDS-PAGE gels. Nanoparticles were reacted with thiolated Flu at a molar ratio of 5:1 pH-responsive NP:Flu to make a Flu−NP conjugate. Antigen conjugation was verified *via* SDS-PAGE (Figure S7A) and gels were imaged with an IVIS Lumina III Imaging System (PerkinElmer, Waltham, MA). DLS was also used to measure the size of Flu−NP conjugates (Figure S7C).

Formation of Nanoparticle/Adjuvant Complexes. NP/adjuvant complexation was carried out by combining CpG ODN 1826 (Invivogen) with NP, OVA−NP, or Flu−NP in PBS at room temperature for at least 30 min. Theoretical charge ratios (+/−) of 4:1 and 6:1 were tested. The charge ratio was defined as the molar ratio between protonated DMAEMA tertiary amines in the first block of the copolymer (positive charge; assuming 50% protonation at physiological pH) and phosphate groups on the CpG backbone (negative charge).[37] The charge ratios at which complete complexation of CpG to the polymer occurred were determined *via* an agarose gel retardation assay (Figure S2B for OVA and Figure S7B for Flu). Free CpG, OVA+CpG, Flu+CpG, and NP/CpG, OVA−NP/CpG, and Flu−NP/CpG complexes prepared at various charge ratios were loaded into lanes of a 4% agarose gel and run at 90 V for 30 min. Gels were stained with GelRed nucleic acid gel stain (Biotium, Fremont, CA) for 20 min and visualized with a Gel Doc EZ system (Bio-Rad). A charge ratio of 6:1 was used for all *in vivo* formulations in order to maximize the stability of the formulation. DLS was used to measure the size of the OVA−NP/CpG formulation (Figure S2C, top right) and Flu−NP/CpG formulation (Figure S7C, bottom), as described above.

Animals. Male or female C57BL/6J mice were purchased from the Jackson Laboratory (Bar Harbor, ME), maintained at the animal facilities of Vanderbilt University under either conventional, specific pathogen-free (SPF barrier facility), or animal biosafety level 2 (ABSL-

DOI: 10.1021/acsnano.9b00326
ACS Nano 2019, 13, 10939−10960

2) conditions, and experimented upon in accordance with the regulations and guidelines of Vanderbilt University Institutional Animal Care and Use Committee (IACUC).

Intranasal Immunization. Endotoxin-free OVA (<1 EU/mg, EndoFit), sterile buffer solutions (1× PBS, pH 7.4), and sterile polymer solutions with ethanol removed were used for vaccine formulations. Experimental groups were as follows: (1) nanoparticles loaded with covalently conjugated OVA and complexed with CpG DNA (OVA−NP/CpG); (2) nanoparticles conjugated to OVA (OVA−NP); (3) a mixture of OVA (nonthiolated) and nanoparticles (OVA+NP); (4) a mixture of CpG-complexed nanoparticles and nonthiolated OVA (NP/CpG+OVA); (5) a mixture of nonthiolated OVA and CpG (OVA+CpG); (6) OVA conjugated to non-pH-responsive control polymer (OVA−NP_{ctrl}); and (7) PBS for sham mice. For all groups containing "NP", this denotes the pH-responsive polymer. Conjugates were prepared 1−2 days before use and stored at 4 °C. OVA was thiolated and used immediately for conjugation to NPs at a molar ratio of 5:1 (NP:OVA), as described above. On the day of use, CpG was complexed to conjugates at a 6:1 charge ratio *via* rapid pipetting of CpG DNA (∼0.5 mg/mL) into the conjugate solution, as described above. The formulation was allowed to react for at least 30 min at room temperature for complete complexation of CpG before administration to mice.

In experiments using OVA antigen, male mice (8−12 weeks old) were anesthetized with ketamine/xylazine (10 mg/mL ketamine hydrochloride, Vedco; 1 mg/mL xylazine hydrochloride, Vanderbilt Pharmacy) by intraperitoneal injection (∼200 μL anesthesia/22 g mouse weight). Anesthetized mice were immunized intranasally on day 0 with formulations containing 7.5 μg of OVA and/or 1.4 μg of CpG with or without 25 μg of polymer. In dosing pilot studies, doses of 50 μg of polymer (15.1 μg of OVA, 2.8 μg of CpG) and 12.5 μg of polymer (3.8 μg of OVA, 0.7 μg of CpG) were also tested; the 25 μg of polymer dose was ultimately selected for its ability to induce a robust $CD8^+$ T cell response with minimal toxicity. Vaccine formulations in a total volume of 80 μL of PBS were delivered *via* pipet through the nostrils into the lungs of mice; inoculation with this volume allows formulations to reach the lower airways.[100] The dose was applied at the center of the nose to allow inhalation into both nostrils, at a rate of ∼8 μL/s. In some cases, anesthetized mice were instead immunized with a subcutaneous injection at the base of the tail. Animals were monitored either daily or three times weekly for weight loss and signs of morbidity.

In experiments using Flu antigen, female mice (10 weeks old) were anesthetized as described and immunized i.n. on day 0 with formulations containing 9.5 μg of Flu and/or 1.4 μg of CpG with or without 25 μg of polymer. Vaccine formulations in a total volume of 80 μL of PBS were delivered through the nostrils as described.

Measurement of Antigen-Specific $CD8^+$ T Cell Response and Tissue-Resident Memory Markers. On days 13, 30, or 60 after immunization, mice were anesthetized and intravenously injected with 200 μL of anti-CD45.2-APC antibody (clone 104; Tonbo) at 0.01 mg/mL (2 μg of αCD45 antibody per mouse), as previously described.[52] This was done to stain marginated vasculature leukocytes (MV; $CD45^+$) and differentiate them from those resident in the lung interstitium (IST; $CD45^-$).[51] To allow for circulation of αCD45 antibody, mice were rested for 3−5 min after i.v. injection and prior to CO_2 euthanasia. For experiments done at day 13, lungs of euthanized mice were perfused with PBS to collect broncheoalveolar lavage fluid from the airway compartment while maintaining IST and MV populations in the lung parenchyma.[52] For day 30 and day 60 experiments, staining with αCXCR3 antibody was used to define airway residence of $CD8^+$ T cells, and lung perfusion was omitted.[52] Lungs and spleens were then collected from each mouse. Organs were harvested and processed as previously described.[101] Briefly, lungs were minced with a scalpel and incubated for 1 h at 37 °C in complete RPMI medium (cRPMI [RPMI+10% FBS]; Gibco) supplemented with 2 mg/mL collagenase (Sigma) and 50 nM dasatinib (LC Laboratories, Woburn, MA). Lungs and spleens were treated with ACK lysing buffer (Gibco) and passed through 70 μm cell strainers to generate single cell suspensions.

Cell suspensions from BAL, lungs, and spleens were stained for 1 h at 4 °C with anti-B220-FITC (clone RA3-6B2; BD Biosciences), anti-CD4-FITC (clone H129.19; BD Biosciences), anti-CD11b-FITC (clone M1/70; Tonbo), anti-CD11c-FITC (clone N418; Tonbo), anti-CD8α-Pacific Blue (clone 53-6.7; BD Biosciences), and 1.5 μg/mL PE-labeled $OVA_{257-264}$ (SIINFEKL)-H-$2K^b$ tetramer (Tet) prepared according to a previously reported procedure.[102] In experiments utilizing mice immunized with Flu antigen, cells were instead stained with PE-labeled $Flu_{366-374}$ (ASNENMETM)-H-$2D^b$ Tet prepared using the same method. Antibodies labeled with FITC (B220/CD4/CD11b/CD11c) were referred to as the "dump" channel and were used to exclude B cells, $CD4^+$ T cells, dendritic cells, and macrophages from gating. In experiments evaluating tissue-resident memory markers on day 30 and day 60, cells from lungs and spleens were also stained with anti-CD69-PE/Cy7 (clone H1.2F3; Tonbo), anti-CD103-Brilliant Violet 510 (clone 2E7; BioLegend), and anti-CXCR3-PerCP/Cy5.5 (clone CXCR3-173; BioLegend). In this case, BAL was not collected, as the number of antigen-specific $CD8^+$ T cells present in BAL samples at these time points is too low for accurate flow cytometric quantification.

After staining, cells were washed with FACS buffer (PBS supplemented with 2% FBS and 50 nM dasatinib) and stained with propidium iodide (BD Biosciences) or Ghost Dye Red 780 (Tonbo) to discriminate live *versus* dead cells. AccuCheck counting beads (Thermo Fisher Scientific) were included in samples to allow for calculation of absolute cell counts. The frequency of antigen-specific $CD8^+$ T cells was determined by flow cytometry on a three-laser LSR-II flow cytometer (BD). All data were analyzed using FlowJo software (version 10.4.2; Tree Star, Inc., Ashland, OR). Cells were gated by forward and side scatter to exclude debris and doublets. Viable antigen-specific $CD8^+$ T cell populations were defined as follows: AW = $CD8\alpha^+CD45^-Tet^+$ cells in BAL samples ($CXCR3^{hi}$ in lung samples for select experiments); IST = $CD8\alpha^+CD45^-Tet^+$ cells in lung samples ($CXCR3^{lo}$ in select experiments); MV = $CD8\alpha^+CD45^+Tet^+$ cells in lung samples; SPL = $CD8\alpha^+Tet^+$ cells in spleen samples. All cells in the $CD8\alpha^+$ gate were also $B220^-CD4^-CD11b^-CD11c^-$ ("dump channel"). T_{RM} cells were defined as either $CD103^+CD69^+$ or $CD103^-CD69^+$ $CD8^+$ T cells in lung samples. Representative gating for each sample type can be found in Figure S3A−C.

Intracellular Cytokine Staining of Antigen-Specific $CD8^+$ T Cells. On day 13 after immunization, lungs and spleens were harvested and processed to obtain single-cell suspensions. Cells were plated in 96-well V-bottom plates at 3×10^6 cells/well (lung) or 2×10^6 cells/well (spleen) in cRPMI and restimulated with 10 μM of MHC class I epitope SIINFEKL peptide ($OVA_{257-264}$; Invivogen). Instead of treatment with peptide, positive controls were treated with PMA (50 ng/mL; Invivogen) and ionomycin (2 μg/mL; Sigma) and negative controls were treated with cRPMI. Cells were incubated at 37 °C and 5% CO2 for 1 h 30 min. BD GolgiPlug protein transport inhibitor (BD Biosciences) was then added to each well and cells were incubated for an additional 5 h 30 min.[37] After incubation, cells were washed with PBS and stained with eFluor 450 fixable viability dye (eBioscience) for 30 min at 4 °C. Cells were next washed with FACS buffer (PBS+2% FBS) and stained with anti-CD8α-APC/Cy7 (clone 53-6.7; Tonbo) and anti-CD3ε-PerCP/Cy5.5 (clone 145−2C11; Tonbo), as well as Fc-block (anti-CD16/CD32, clone 2.4G2; Tonbo), for 1 h at 4 °C. Cells were washed 2× in FACS buffer, then fixed and permeabilized by incubating for 10 min at 4 °C with BD Cytofix/Cytoperm (BD Biosciences), according to manufacturer instructions. Cells were then washed 2× with 1× BD perm/wash buffer (BD Biosciences) and incubated for 1 h at 4 °C with antibodies against intracellular cytokines: anti-IFNγ-APC (clone XMG1.2; BD Biosciences) and anti-TNFα-PE (clone MP6-XT22; BD Biosciences). Finally, cells were washed once with 1× perm/wash buffer, resuspended in FACS buffer supplemented with 50 nM dasatinib, and analyzed by flow cytometry using a three-laser LSR-II flow cytometer (BD) and FlowJo software (v.10.4.2). Data are reported as the percentage of $CD8\alpha^+CD3\varepsilon^+$ cells that are $IFN\gamma^+$ and/or $TNF\alpha^+$ after subtraction of background values from negative (unstimulated) controls. Representative gating for lungs and spleens can found in Figure S3D.

DOI: 10.1021/acsnano.9b00326
ACS Nano 2019, 13, 10939−10960

Histology. Lungs from mice immunized with OVA−NP/CpG or OVA+CpG, or from untreated mice, were harvested on day 1 and day 12 postimmunization. Tissue was fixed in 10% neutral buffered formalin, processed routinely, sectioned at 5 μm, and stained with hematoxylin and eosin (H&E). Sections were evaluated by an experienced veterinary pathologist blinded to the composition of the groups. Representative images are provided in Figure S4B.

Fluorescence Microscopy. Mice were immunized i.n. with antigen−NP conjugates containing OVA labeled with Alexa Fluor 647 (OVA_{647}-NP). After 24 h, mice were injected i.v. with anti-CD45-Brilliant Violet 421 antibody (clone 30-F11; BD Biosciences) and Alexa Fluor 488-labeled tomato lectin (Vector Laboratories) to visualize intravascular lung leukocytes and vasculature, respectively.

Mice were euthanized, and lungs were harvested and fixed by inflation with 1 mL of 4% paraformaldehyde followed by 15% sucrose administered through the trachea. Lungs were frozen in OCT (Fisher Scientific). Ten micrometer tissue sections were evaluated by fluorescence microscopy using an Axioplan wide-field microscope (Zeiss) equipped with a 20× objective, 405, 488, 532, and 633 nm laser lines, and a Hamamatsu ORCA-ER monochrome digital camera.

Uptake and Activation in Pulmonary Innate Immune Cells. To identify the effects of the NP vaccine on innate immune cell uptake and activation in lungs, mice were immunized with fluorescently labeled OVA_{647}-NP/CpG_{488} or OVA_{647}+CpG_{488}, or with PBS (control). In the fluorescent formulations, OVA was labeled with Alexa Fluor 647 as described above (OVA_{647}). Alexa Fluor 488-labeled CpG (CpG_{488}) was purchased from Integrated DNA Technologies (IDT; Skokie, IL). After 24, 48, or 72 h, mice were euthanized and lungs were harvested, as well as spleens (to assess systemic biodistribution). Organs were imaged using an IVIS Lumina III Imaging System (PerkinElmer, Waltham, MA) to visualize and quantify tissue-level OVA_{647} fluorescence after immunization. IVIS image files were analyzed using Living Image software (version 4.5.5, PerkinElmer).

After imaging, lungs were processed as described above to obtain single-cell suspensions. Lung samples were stained for flow cytometric analysis of pulmonary immune cells using a modified version of the panel described by Misharin *et al.*[58] This panel was used to distinguish seven different cell types: (1) alveolar macrophages (AMφ); (2) interstitial macrophages (IMφ); (3) $CD103^+$ dendritic cells ($CD103^+$DC); (4) $CD11b^+$ dendritic cells ($CD11b^+$DC); (5) monocytes/macrophages (Mono/Mφ); (6) granulocytes (Gran); and (7) cells not included in other populations (other). It was also used to quantify the amount of cargo colocalization (OVA^+CpG^+ cells) and expression of activation marker CD86 in each cell subset and at each time point. The following antibodies were used: anti-CD64-PE (BioLegend; X54−5/7.1), anti-CD24-PE/Cy7 (BioLegend; M1/69), anti-CD11b-PerCP/Cy5.5 (BioLegend; M1/70), anti-CD11c-APC/Cy7 (Tonbo; N418), anti-I-A/I-E-Brilliant Violet 605 (BD; M5/114.15.2), anti-CD45.2-Brilliant Violet 650 (BioLegend; 104), and anti-CD86-PE/Dazzle 594 (BioLegend; GL-1). Ghost Dye Violet 510 (Tonbo) was used to discriminate live *versus* dead cells and AccuCheck counting beads (Thermo Fisher Scientific) were included in samples to allow for calculation of absolute cell counts. Samples were stained with viability dye for 30 min at 4 °C, washed with FACS buffer (PBS+2% FBS, 50 nM dasatinib), incubated with Fc-block (anti-CD16/CD32, clone 2.4G2; Tonbo) for 15 min at 4 °C, and then stained for 1 h at 4 °C with the antibody panel listed above. Finally, cells were washed once, resuspended in FACS buffer, and analyzed by flow cytometry. Data were collected using a three-laser Fortessa (BD) and analyzed with FlowJo software (v.10.4.2). Representative gating for OVA and CpG uptake in lung cell subsets can be found in Figure S5.

Measurement of Cytokines. Cytokines were measured in serum, BAL, or lung homogenates using a LEGENDplex bead-based immunoassay (BioLegend). Mice were immunized i.n. and blood, BAL, and lungs were harvested 6 h, 24 h, 48 h, and 7 d after immunization. Blood was obtained by cardiac puncture and BAL was collected by lavage with 1 mL sterile PBS containing a cocktail of protease inhibitors (Roche cOmplete Mini EDTA-free Protease Inhibitor Cocktail, Sigma). The right sides (4 lobes) of lungs were collected in 1 mL M-PER Mammalian Protein Extraction Reagent (Thermo Fisher Scientific) with protease inhibitors and homogenized using a gentleMACS Octo Dissociator and M tubes (Miltenyi Biotec), according to manufacturer instructions. Lung homogenates were then centrifuged for 10 min at 4200 rpm and supernatants were collected and frozen at −80 °C until analysis. BAL samples were frozen at −80 °C without further processing. Blood was centrifuged for 10 min at 14 000 rpm (2×), and sera were collected and frozen at −80 °C until analysis. Prior to use with LEGENDplex kits, samples were thawed and centrifuged for 10 min at 10 000−12 500 rpm to remove debris. Lung samples were filtered through 40 μm cell strainers for additional debris removal. The following cytokines were measured: IFNγ, TNFα, IFNα, IFNβ, IL-6, IL-33, IL-12p70, and IL-1β. LEGENDplex kits were used according to manufacturer instructions. Flow cytometric data were collected with a three-laser LSR II (BD) and analyzed with LEGENDplex data analysis software (v.8.0).

Vaccinia Virus Propagation, Intranasal Virus Challenge, and Lung Burden. Recombinant vaccinia virus expressing influenza virus nucleoprotein, ovalbumin SIINFEKL peptide, and enhanced green fluorescent protein (VV.NP-S-EGFP) was obtained through the NIH Biodefense and Emerging Infections Research Resources Repository, NIAID, NIH (NR-624; BEI Resources, Manassas, VA). The virus was grown in HeLa cells and titrated using BSC-40 cells. For titration, crystal violet stain (Eng Scientific, Clifton, NJ) was used to visualize plaques 48 h after applying serial 10-fold dilutions of the virus in HBSS +0.5% (w/v) BSA to confluent monolayers of BSC-40 cells.

For respiratory virus challenge, 10 to 16 week old immunized male mice were anesthetized i.v. with ketamine/xylazine as described above and inoculated i.n. with a sublethal dose (1×10^7 pfu) of virus in 80 μL of sterile PBS. Mice were monitored daily for morbidity and weight loss. On day 6 postinfection, lungs from individual mice were harvested into 2 mL of HBSS (supplemented with 0.5% (w/v) BSA and 1× pen/strep, sterilized by vacuum filtration) and frozen at −80 °C.

To determine viral burden using a plaque assay, previously frozen lungs were thawed, homogenized in HBSS using a Tissue Tearor (BioSpec Products, Bartlesville, OK), and subjected to one additional freeze−thaw cycle. Serial 10-fold dilutions of lung homogenates were plated on confluent monolayers of BSC-40 cells. After 48 h, plaques were visualized by crystal violet staining.

Influenza A Virus Challenge. Influenza A virus (strain A/Puerto Rico/8/1934, subtype H1N1) (PR8) was obtained through BEI Resources, NIAID, NIH (NR-348; Manassas, VA). For respiratory virus challenge, 14 to 18 week old immunized female mice were anesthetized i.v. with ketamine/xylazine as described above and inoculated i.n. with a lethal dose (200 FFU) of virus in 80 μL of sterile PBS. Mice were monitored daily through day 14 postinfection for morbidity, weight loss, and survival. After infection, mice were euthanized when weight loss exceeded 30% of initial body weight, in accordance with IACUC guidelines.

Statistical Analysis. Statistical analyses were performed as indicated in figure legends. All analyses were done using GraphPad Prism software, version 6.07. Results are expressed as mean ± SEM with $^{****}p < 0.0001$, $^{***}p < 0.001$, $^{**}p < 0.01$, $^{*}p < 0.05$ being considered statistically significant.

ASSOCIATED CONTENT

Supporting Information

The Supporting Information is available free of charge on the ACS Publications website at DOI: 10.1021/acsnano.9b00326.

Supplementary figures detailing polymer, nanoparticle, and conjugate/complex characterization; flow cytometry gating strategies; weight loss and lung histology after immunization; additional uptake and cytokine profile data; and polymer synthesis schema (PDF)

AUTHOR INFORMATION

Corresponding Author

*E-mail: john.t.wilson@vanderbilt.edu.

DOI: 10.1021/acsnano.9b00326
ACS Nano 2019, 13, 10939−10960

ORCID

Frances C. Knight: 0000-0001-8892-7262
Kyle W. Becker: 0000-0003-1627-2724
James E. Crowe, Jr.: 0000-0002-0049-1079
John T. Wilson: 0000-0002-9144-2634

Author Contributions

Conceptualization was done by F.C.K., P.G., S.J., and J.T.W.; methodology was done by F.C.K., P.G., A.K., S.J., and J.T.W.; formal analysis was done by F.C.K. and P.G.; F.C.K., P.G., A.K., K.W.B., S.S., M.J., L.W.-B., and K.L.B. performed experiments; resources were provided by N.S., K.L.B., J.E.C., S.J., J.T.W.; F.C.K. wrote the original draft; F.C.K., P.G., J.E.C., S.J., and J.T.W. were responsible for reviewing and editing the manuscript; data visualization and figure preparation was done by F.C.K.; S.J. and J.T.W. supervised; S.J. and J.T.W. were responsible for funding acquisition.

Notes

The authors declare the following competing financial interest(s): J.E.C. has served as a consultant for Takeda Vaccines, Sanofi Pasteur, Pfizer, and Novavax, is on the Scientific Advisory Boards of CompuVax, GigaGen, and Meissa Vaccines, and is Founder of IDBiologics, Inc. The other authors declare no competing interests.

ACKNOWLEDGMENTS

We thank the Duvall lab (Vanderbilt) for the use of GPC and IVIS imaging equipment; the core facilities of the Vanderbilt Institute of Nanoscale Science and Engineering for use of DLS equipment; the Vanderbilt Translational Pathology Shared Resource for histological analysis; and the VUMC Flow Cytometry Shared Resource, supported by the Vanderbilt Ingram Cancer Center (P30 CA68485) and the Vanderbilt Digestive Disease Research Center (DK058404) for use of flow cytometry equipment. The following reagents were obtained through BEI Resources, NIAID, NIH: Vaccinia Virus, VV.NP-S-EGFP, recombinant expressing enhanced green fluorescent protein (NR-624) and Influenza A Virus, A/Puerto Rico/8/1934 (H1N1) (NR-348). This research was supported by NIH 5R21AI121626 (J.T.W.), NIH HL121139 (S.J.), NSF CBET-1554623 (J.T.W.), Vanderbilt University Discovery Grant Program (J.T.W., S.J.), Vanderbilt University School of Engineering (J.T.W.), Veteran's Affairs Merit Award BX001444 (S.J.), and also supported by a Stand Up To Cancer Innovative Research Grant, Grant No. SU2C-AACR-IRG 20-17 (J.T.W.). Stand Up To Cancer (SU2C) is a program of the Entertainment Industry Foundation. Research grants are administered by the American Association for Cancer Research, the scientific partner of SU2C.

REFERENCES

(1) Gebhardt, T.; Palendira, U.; Tscharke, D. C.; Bedoui, S. Tissue-Resident Memory T Cells in Tissue Homeostasis, Persistent Infection, and Cancer Surveillance. *Immunol. Rev.* **2018**, *283*, 54−76.

(2) Schenkel, J. M.; Masopust, D. Tissue-Resident Memory T Cells. *Immunity* **2014**, *41*, 886−897.

(3) Shin, H.; Iwasaki, A. Tissue-Resident Memory T Cells. *Immunol. Rev.* **2013**, *255*, 165−181.

(4) Mueller, S. N.; Gebhardt, T.; Carbone, F. R.; Heath, W. R. Memory T Cell Subsets, Migration Patterns, and Tissue Residence. *Annu. Rev. Immunol.* **2013**, *31*, 137−161.

(5) Ariotti, S.; Haanen, J. B.; Schumacher, T. N. Behavior and Function of Tissue-Resident Memory T Cells. *Adv. Immunol.* **2012**, *114*, 203−216.

(6) Buggert, M.; Nguyen, S.; Salgado-Montes de Oca, G.; Bengsch, B.; Darko, S.; Ransier, A.; Roberts, E. R.; Del Alcazar, D.; Brody, I. B.; Vella, L. A.; Beura, L.; Wijeyesinghe, S.; Herati, R. S.; Del Rio Estrada, P. M.; Ablanedo-Terrazas, Y.; Kuri-Cervantes, L.; Sada Japp, A.; Manne, S.; Vartanian, S.; Huffman, A.; et al. Identification and Characterization of HIV-Specific Resident Memory CD8(+) T Cells in Human Lymphoid Tissue. *Sci. Immunol.* **2018**, *3*, No. eaar4526.

(7) Haddadi, S.; Thanthrige-Don, N.; Afkhami, S.; Khera, A.; Jeyanathan, M.; Xing, Z. Expression and Role of VLA-1 in Resident Memory CD8 T Cell Responses to Respiratory Mucosal Viral-Vectored Immunization against Tuberculosis. *Sci. Rep.* **2017**, *7*, 9525.

(8) Jozwik, A.; Habibi, M. S.; Paras, A.; Zhu, J.; Guvenel, A.; Dhariwal, J.; Almond, M.; Wong, E. H.; Sykes, A.; Maybeno, M.; Del Rosario, J.; Trujillo-Torralbo, M. B.; Mallia, P.; Sidney, J.; Peters, B.; Kon, O. M.; Sette, A.; Johnston, S. L.; Openshaw, P. J.; Chiu, C. RSV-Specific Airway Resident Memory CD8+ T Cells and Differential Disease Severity after Experimental Human Infection. *Nat. Commun.* **2015**, *6*, 10224.

(9) Laidlaw, B. J.; Zhang, N.; Marshall, H. D.; Staron, M. M.; Guan, T.; Hu, Y.; Cauley, L. S.; Craft, J.; Kaech, S. M. CD4+ T Cell Help Guides Formation of CD103+ Lung-Resident Memory CD8+ T Cells During Influenza Viral Infection. *Immunity* **2014**, *41*, 633−645.

(10) Savas, P.; Virassamy, B.; Ye, C.; Salim, A.; Mintoff, C. P.; Caramia, F.; Salgado, R.; Byrne, D. J.; Teo, Z. L.; Dushyanthen, S.; Byrne, A.; Wein, L.; Luen, S. J.; Poliness, C.; Nightingale, S. S.; Skandarajah, A. S.; Gyorki, D. E.; Thornton, C. M.; Beavis, P. A.; Fox, S. B.; et al. Single-Cell Profiling of Breast Cancer T Cells Reveals a Tissue-Resident Memory Subset Associated with Improved Prognosis. *Nat. Med.* **2018**, *24*, 986−993.

(11) Enamorado, M.; Iborra, S.; Priego, E.; Cueto, F. J.; Quintana, J. A.; Martinez-Cano, S.; Mejias-Perez, E.; Esteban, M.; Melero, I.; Hidalgo, A.; Sancho, D. Enhanced Anti-Tumour Immunity Requires the Interplay between Resident and Circulating Memory CD8(+) T Cells. *Nat. Commun.* **2017**, *8*, 16073.

(12) Djenidi, F.; Adam, J.; Goubar, A.; Durgeau, A.; Meurice, G.; de Montpreville, V.; Validire, P.; Besse, B.; Mami-Chouaib, F. CD8+CD103+ Tumor-Infiltrating Lymphocytes Are Tumor-Specific Tissue-Resident Memory T Cells and a Prognostic Factor for Survival in Lung Cancer Patients. *J. Immunol.* **2015**, *194*, 3475−3486.

(13) Nizard, M.; Roussel, H.; Diniz, M. O.; Karaki, S.; Tran, T.; Voron, T.; Dransart, E.; Sandoval, F.; Riquet, M.; Rance, B.; Marcheteau, E.; Fabre, E.; Mandavit, M.; Terme, M.; Blanc, C.; Escudie, J. B.; Gibault, L.; Barthes, F. L. P.; Granier, C.; Ferreira, L. C. S.; et al. Induction of Resident Memory T Cells Enhances the Efficacy of Cancer Vaccine. *Nat. Commun.* **2017**, *8*, 15221.

(14) Sakai, S.; Kauffman, K. D.; Schenkel, J. M.; McBerry, C. C.; Mayer-Barber, K. D.; Masopust, D.; Barber, D. L. Cutting Edge: Control of Mycobacterium Tuberculosis Infection by a Subset of Lung Parenchyma-Homing CD4 T Cells. *J. Immunol.* **2014**, *192*, 2965−2969.

(15) Pizzolla, A.; Nguyen, T. H.; Sant, S.; Jaffar, J.; Loudovaris, T.; Mannering, S. I.; Thomas, P. G.; Westall, G. P.; Kedzierska, K.; Wakim, L. M. Influenza-Specific Lung-Resident Memory T Cells Are Proliferative and Polyfunctional and Maintain Diverse TCR Profiles. *J. Clin. Invest.* **2018**, *128*, 721−733.

(16) Park, S. L.; Buzzai, A.; Rautela, J.; Hor, J. L.; Hochheiser, K.; Effern, M.; McBain, N.; Wagner, T.; Edwards, J.; McConville, R.; Wilmott, J. S.; Scolyer, R. A.; Tuting, T.; Palendira, U.; Gyorki, D.; Mueller, S. N.; Huntington, N. D.; Bedoui, S.; Holzel, M.; Mackay, L. K.; et al. Tissue-Resident Memory CD8(+) T Cells Promote Melanoma-Immune Equilibrium in Skin. *Nature* **2019**, *565*, 366−371.

(17) Wu, T.; Hu, Y.; Lee, Y. T.; Bouchard, K. R.; Benechet, A.; Khanna, K.; Cauley, L. S. Lung-Resident Memory CD8 T Cells (Trm) Are Indispensable for Optimal Cross-Protection against Pulmonary Virus Infection. *J. Leukocyte Biol.* **2014**, *95*, 215−224.

(18) Zens, K. D.; Chen, J. K.; Farber, D. L. Vaccine-Generated Lung Tissue-Resident Memory T Cells Provide Heterosubtypic Protection to Influenza Infection. *JCI Insight* **2016**, *1*, No. e85832.

(19) Perdomo, C.; Zedler, U.; Kuhl, A. A.; Lozza, L.; Saikali, P.; Sander, L. E.; Vogelzang, A.; Kaufmann, S. H.; Kupz, A. Mucosal BCG

DOI: 10.1021/acsnano.9b00326
ACS Nano 2019, 13, 10939−10960

Vaccination Induces Protective Lung-Resident Memory T Cell Populations against Tuberculosis. *mBio* **2016**, *7*, No. e01686.
(20) Takamura, S.; Yagi, H.; Hakata, Y.; Motozono, C.; McMaster, S. R.; Masumoto, T.; Fujisawa, M.; Chikaishi, T.; Komeda, J.; Itoh, J.; Umemura, M.; Kyusai, A.; Tomura, M.; Nakayama, T.; Woodland, D. L.; Kohlmeier, J. E.; Miyazawa, M. Specific Niches for Lung-Resident Memory CD8+ T Cells at the Site of Tissue Regeneration Enable CD69-Independent Maintenance. *J. Exp. Med.* **2016**, *213*, 3057−3073.
(21) McMaster, S. R.; Wilson, J. J.; Wang, H.; Kohlmeier, J. E. Airway-Resident Memory CD8 T Cells Provide Antigen-Specific Protection against Respiratory Virus Challenge through Rapid IFN-Gamma Production. *J. Immunol.* **2015**, *195*, 203−209.
(22) Kinnear, E.; Lambert, L.; McDonald, J. U.; Cheeseman, H. M.; Caproni, L. J.; Tregoning, J. S. Airway T Cells Protect against RSV Infection in the Absence of Antibody. *Mucosal Immunol.* **2018**, *11*, 249−256.
(23) Neutra, M. R.; Kozlowski, P. A. Mucosal Vaccines: The Promise and the Challenge. *Nat. Rev. Immunol.* **2006**, *6*, 148−158.
(24) Lapuente, D.; Storcksdieck Genannt Bonsmann, M.; Maaske, A.; Stab, V.; Heinecke, V.; Watzstedt, K.; Hess, R.; Westendorf, A. M.; Bayer, W.; Ehrhardt, C.; Tenbusch, M. IL-1beta as Mucosal Vaccine Adjuvant: The Specific Induction of Tissue-Resident Memory T Cells Improves the Heterosubtypic Immunity against Influenza a Viruses. *Mucosal Immunol.* **2018**, *11*, 1265−1278.
(25) Morabito, K. M.; Ruckwardt, T. J.; Bar-Haim, E.; Nair, D.; Moin, S. M.; Redwood, A. J.; Price, D. A.; Graham, B. S. Memory Inflation Drives Tissue-Resident Memory CS8(+) T Cell Maintenance in the Lung after Intranasal Vaccination with Murine Cytomegalovirus. *Front. Immunol.* **2018**, *9*, 1861.
(26) Li, A. V.; Moon, J. J.; Abraham, W.; Suh, H.; Elkhader, J.; Seidman, M. A.; Yen, M.; Im, E. J.; Foley, M. H.; Barouch, D. H.; Irvine, D. J. Generation of Effector Memory T Cell-Based Mucosal and Systemic Immunity with Pulmonary Nanoparticle Vaccination. *Sci. Transl. Med.* **2013**, *5*, 204ra130.
(27) Woodrow, K. A.; Bennett, K. M.; Lo, D. D. Mucosal Vaccine Design and Delivery. *Annu. Rev. Biomed. Eng.* **2012**, *14*, 17−46.
(28) Yewdell, J. W. Designing CD8+ T Cell Vaccines: It's Not Rocket Science (Yet). *Curr. Opin. Immunol.* **2010**, *22*, 402−410.
(29) Perrie, Y.; Mohammed, A. R.; Kirby, D. J.; McNeil, S. E.; Bramwell, V. W. Vaccine Adjuvant Systems: Enhancing the Efficacy of Sub-Unit Protein Antigens. *Int. J. Pharm.* **2008**, *364*, 272−280.
(30) Foged, C.; Hansen, J.; Agger, E. M. License to Kill: Formulation Requirements for Optimal Priming of CD8(+) CTL Responses with Particulate Vaccine Delivery Systems. *Eur. J. Pharm. Sci.* **2012**, *45*, 482−491.
(31) Swartz, M. A.; Hirosue, S.; Hubbell, J. A. Engineering Approaches to Immunotherapy. *Sci. Transl. Med.* **2012**, *4*, 148rv9.
(32) Koup, R. A.; Douek, D. C. Vaccine Design for CD8 T Lymphocyte Responses. *Cold Spring Harbor Perspect. Med.* **2011**, *1*, a007252.
(33) Foged, C. Subunit Vaccines of the Future: The Need for Safe, Customized and Optimized Particulate Delivery Systems. *Ther. Delivery* **2011**, *2*, 1057−1077.
(34) Bookstaver, M. L.; Tsai, S. J.; Bromberg, J. S.; Jewell, C. M. Improving Vaccine and Immunotherapy Design Using Biomaterials. *Trends Immunol.* **2018**, *39*, 135−150.
(35) Sahdev, P.; Ochyl, L. J.; Moon, J. J. Biomaterials for Nanoparticle Vaccine Delivery Systems. *Pharm. Res.* **2014**, *31*, 2563−2582.
(36) Stano, A.; Scott, E. A.; Dane, K. Y.; Swartz, M. A.; Hubbell, J. A. Tunable T Cell Immunity Towards a Protein Antigen Using Polymersomes *vs.* Solid-Core Nanoparticles. *Biomaterials* **2013**, *34*, 4339−4346.
(37) Wilson, J. T.; Keller, S.; Manganiello, M. J.; Cheng, C.; Lee, C. C.; Opara, C.; Convertine, A.; Stayton, P. S. pH-Responsive Nanoparticle Vaccines for Dual-Delivery of Antigens and Immunostimulatory Oligonucleotides. *ACS Nano* **2013**, *7*, 3912−3925.
(38) Kapadia, C. H.; Tian, S.; Perry, J. L.; Sailer, D.; Christopher Luft, J.; DeSimone, J. M. Extending Antigen Release from Particulate Vaccines Results in Enhanced Antitumor Immune Response. *J. Controlled Release* **2018**, *269*, 393−404.
(39) de Titta, A.; Ballester, M.; Julier, Z.; Nembrini, C.; Jeanbart, L.; van der Vlies, A. J.; Swartz, M. A.; Hubbell, J. A. Nanoparticle Conjugation of CpG Enhances Adjuvancy for Cellular Immunity and Memory Recall at Low Dose. *Proc. Natl. Acad. Sci. U. S. A.* **2013**, *110*, 19902−19907.
(40) Nembrini, C.; Stano, A.; Dane, K. Y.; Ballester, M.; van der Vlies, A. J.; Marsland, B. J.; Swartz, M. A.; Hubbell, J. A. Nanoparticle Conjugation of Antigen Enhances Cytotoxic T-Cell Responses in Pulmonary Vaccination. *Proc. Natl. Acad. Sci. U. S. A.* **2011**, *108*, E989−997.
(41) Qiu, F.; Becker, K. W.; Knight, F. C.; Baljon, J. J.; Sevimli, S.; Shae, D.; Gilchuk, P.; Joyce, S.; Wilson, J. T. Poly(Propylacrylic Acid)-Peptide Nanoplexes as a Platform for Enhancing the Immunogenicity of Neoantigen Cancer Vaccines. *Biomaterials* **2018**, *182*, 82−91.
(42) Ballester, M.; Nembrini, C.; Dhar, N.; de Titta, A.; de Piano, C.; Pasquier, M.; Simeoni, E.; van der Vlies, A. J.; McKinney, J. D.; Hubbell, J. A.; Swartz, M. A. Nanoparticle Conjugation and Pulmonary Delivery Enhance the Protective Efficacy of Ag85B and CpG against Tuberculosis. *Vaccine* **2011**, *29*, 6959−6966.
(43) Si, Y.; Wen, Y.; Kelly, S. H.; Chong, A. S.; Collier, J. H. Intranasal Delivery of Adjuvant-Free Peptide Nanofibers Elicits Resident CD8(+) T Cell Responses. *J. Controlled Release* **2018**, *282*, 120−130.
(44) Zacharias, Z. R.; Ross, K. A.; Hornick, E. E.; Goodman, J. T.; Narasimhan, B.; Waldschmidt, T. J.; Legge, K. L. Polyanhydride Nanovaccine Induces Robust Pulmonary B and T Cell Immunity and Confers Protection against Homologous and Heterologous Influenza A Virus Infections. *Front. Immunol.* **2018**, *9*, 1953.
(45) Wakim, L. M.; Gupta, N.; Mintern, J. D.; Villadangos, J. A. Enhanced Survival of Lung Tissue-Resident Memory CD8(+) T Cells During Infection with Influenza Virus Due to Selective Expression of IFITM3. *Nat. Immunol.* **2013**, *14*, 238−245.
(46) Coffman, R. L.; Sher, A.; Seder, R. A. Vaccine Adjuvants: Putting Innate Immunity to Work. *Immunity* **2010**, *33*, 492−503.
(47) McMaster, S. R.; Wein, A. N.; Dunbar, P. R.; Hayward, S. L.; Cartwright, E. K.; Denning, T. L.; Kohlmeier, J. E. Pulmonary Antigen Encounter Regulates the Establishment of Tissue-Resident CD8Memory T Cells in the Lung Airways and Parenchyma. *Mucosal Immunol.* **2018**, *11*, 1071−1078.
(48) Kim, T. S.; Hufford, M. M.; Sun, J.; Fu, Y. X.; Braciale, T. J. Antigen Persistence and the Control of Local T Cell Memory by Migrant Respiratory Dendritic Cells after Acute Virus Infection. *J. Exp. Med.* **2010**, *207*, 1161−1172.
(49) Ho, N. I.; Huis In 't Veld, L. G. M.; Raaijmakers, T. K.; Adema, G. J. Adjuvants Enhancing Cross-Presentation by Dendritic Cells: The Key to More Effective Vaccines? *Front. Immunol.* **2018**, *9*, 2874.
(50) Anderson, K. G.; Sung, H.; Skon, C. N.; Lefrancois, L.; Deisinger, A.; Vezys, V.; Masopust, D. Cutting Edge: Intravascular Staining Redefines Lung CD8 T Cell Responses. *J. Immunol.* **2012**, *189*, 2702−2706.
(51) Anderson, K. G.; Mayer-Barber, K.; Sung, H.; Beura, L.; James, B. R.; Taylor, J. J.; Qunaj, L.; Griffith, T. S.; Vezys, V.; Barber, D. L.; Masopust, D. Intravascular Staining for Discrimination of Vascular and Tissue Leukocytes. *Nat. Protoc.* **2014**, *9*, 209−222.
(52) Gilchuk, P.; Hill, T. M.; Guy, C.; McMaster, S. R.; Boyd, K. L.; Rabacal, W. A.; Lu, P.; Shyr, Y.; Kohlmeier, J. E.; Sebzda, E.; Green, D. R.; Joyce, S. A Distinct Lung-Interstitium-Resident Memory CD8(+) T Cell Subset Confers Enhanced Protection to Lower Respiratory Tract Infection. *Cell Rep.* **2016**, *16*, 1800−1809.
(53) Riehn, M.; Cebula, M.; Hauser, H.; Wirth, D. CpG-ODN Facilitates Effective Intratracheal Immunization and Recall of Memory against Neoantigen-Expressing Alveolar Cells. *Front. Immunol.* **2017**, *8*, 1201.
(54) Khan, T. N.; Mooster, J. L.; Kilgore, A. M.; Osborn, J. F.; Nolz, J. C. Local Antigen in Nonlymphoid Tissue Promotes Resident Memory CD8+ T Cell Formation During Viral Infection. *J. Exp. Med.* **2016**, *213*, 951−966.

DOI: 10.1021/acsnano.9b00326
ACS Nano 2019, 13, 10939−10960

(55) Wakim, L. M.; Smith, J.; Caminschi, I.; Lahoud, M. H.; Villadangos, J. A. Antibody-Targeted Vaccination to Lung Dendritic Cells Generates Tissue-Resident Memory CD8 T Cells That Are Highly Protective against Influenza Virus Infection. *Mucosal Immunol.* **2015**, *8*, 1060−1071.
(56) Iborra, S.; Martinez-Lopez, M.; Khouili, S. C.; Enamorado, M.; Cueto, F. J.; Conde-Garrosa, R.; Del Fresno, C.; Sancho, D. Optimal Generation of Tissue-Resident but Not Circulating Memory T Cells During Viral Infection Requires Crosspriming by DNGR-1(+) Dendritic Cells. *Immunity* **2016**, *45*, 847−860.
(57) Macdonald, D. C.; Singh, H.; Whelan, M. A.; Escors, D.; Arce, F.; Bottoms, S. E.; Barclay, W. S.; Maini, M.; Collins, M. K.; Rosenberg, W. M. Harnessing Alveolar Macrophages for Sustained Mucosal T-Cell Recall Confers Long-Term Protection to Mice against Lethal Influenza Challenge without Clinical Disease. *Mucosal Immunol.* **2014**, *7*, 89−100.
(58) Misharin, A. V.; Morales-Nebreda, L.; Mutlu, G. M.; Budinger, G. R.; Perlman, H. Flow Cytometric Analysis of Macrophages and Dendritic Cell Subsets in the Mouse Lung. *Am. J. Respir. Cell Mol. Biol.* **2013**, *49*, 503−510.
(59) Topham, D. J.; Reilly, E. C. Tissue-Resident Memory CD8(+) T Cells: From Phenotype to Function. *Front. Immunol.* **2018**, *9*, 515.
(60) Amsen, D.; van Gisbergen, K.; Hombrink, P.; van Lier, R. A. W. Tissue-Resident Memory T Cells at the Center of Immunity to Solid Tumors. *Nat. Immunol.* **2018**, *19*, 538−546.
(61) Masopust, D.; Vezys, V.; Wherry, E. J.; Barber, D. L.; Ahmed, R. Cutting Edge: Gut Microenvironment Promotes Differentiation of a Unique Memory CD8 T Cell Population. *J. Immunol.* **2006**, *176*, 2079−2083.
(62) Mackay, L. K.; Rahimpour, A.; Ma, J. Z.; Collins, N.; Stock, A. T.; Hafon, M. L.; Vega-Ramos, J.; Lauzurica, P.; Mueller, S. N.; Stefanovic, T.; Tscharke, D. C.; Heath, W. R.; Inouye, M.; Carbone, F. R.; Gebhardt, T. The Developmental Pathway for CD103(+)CD8(+) Tissue-Resident Memory T Cells of Skin. *Nat. Immunol.* **2013**, *14*, 1294−1301.
(63) Ben-Sasson, S. Z.; Hogg, A.; Hu-Li, J.; Wingfield, P.; Chen, X.; Crank, M.; Caucheteux, S.; Ratner-Hurevich, M.; Berzofsky, J. A.; Nir-Paz, R.; Paul, W. E. E. IL-1 Enhances Expansion, Effector Function, Tissue Localization, and Memory Response of Antigen-Specific CD8 T Cells. *J. Exp. Med.* **2013**, *210*, 491−502.
(64) Cox, M. A.; Harrington, L. E.; Zajac, A. J. Cytokines and the Inception of CD8 T Cell Responses. *Trends Immunol.* **2011**, *32*, 180−186.
(65) Curtsinger, J. M.; Agarwal, P.; Lins, D. C.; Mescher, M. F. Autocrine IFN-Gamma Promotes Naive CD8 T Cell Differentiation and Synergizes with IFN-Alpha to Stimulate Strong Function. *J. Immunol.* **2012**, *189*, 659−668.
(66) Henry, C. J.; Ornelles, D. A.; Mitchell, L. M.; Brzoza-Lewis, K. L.; Hiltbold, E. M. IL-12 Produced by Dendritic Cells Augments CD8+ T Cell Activation through the Production of the Chemokines CCL1 and CCL17. *J. Immunol.* **2008**, *181*, 8576−8584.
(67) Lee, Y. J.; Won, T. J.; Hyung, K. E.; Jang, Y. W.; Kim, S. J.; Lee, D. I.; Park, S. Y.; Hwang, K. W. IL-6 Induced Proliferation and Cytotoxic Activity of CD8(+) T Cells Is Elevated by SUMO2 Overexpression. *Arch. Pharmacal Res.* **2016**, *39*, 705−712.
(68) Skon, C. N.; Lee, J. Y.; Anderson, K. G.; Masopust, D.; Hogquist, K. A.; Jameson, S. C. Transcriptional Downregulation of S1PR1 Is Required for the Establishment of Resident Memory CD8+ T Cells. *Nat. Immunol.* **2013**, *14*, 1285−1293.
(69) Fromen, C. A.; Rahhal, T. B.; Robbins, G. R.; Kai, M. P.; Shen, T. W.; Luft, J. C.; DeSimone, J. M. Nanoparticle Surface Charge Impacts Distribution, Uptake and Lymph Node Trafficking by Pulmonary Antigen-Presenting Cells. *Nanomedicine* **2016**, *12*, 677−687.
(70) Pesce, I.; Monaci, E.; Muzzi, A.; Tritto, E.; Tavarini, S.; Nuti, S.; De Gregorio, E.; Wack, A. Intranasal Administration of CpG Induces a Rapid and Transient Cytokine Response Followed by Dendritic and Natural Killer Cell Activation and Recruitment in the Mouse Lung. *J. Innate Immun.* **2010**, *2*, 144−159.
(71) Slutter, B.; Pewe, L. L.; Kaech, S. M.; Harty, J. T. Lung Airway-Surveilling CXCR3(hi) Memory CD8(+) T Cells Are Critical for Protection against Influenza A Virus. *Immunity* **2013**, *39*, 939−948.
(72) Bailey, E. S.; Choi, J. Y.; Fieldhouse, J. K.; Borkenhagen, L. K.; Zemke, J.; Zhang, D.; Gray, G. C. The Continual Threat of Influenza Virus Infections at the Human-Animal Interface: What Is New from a One Health Perspective? *Evol. Med. Public Health* **2018**, *2018*, 192−198.
(73) Li, Z. T.; Zarnitsyna, V. I.; Lowen, A. C.; Weissman, D.; Koelle, K.; Kohlmeier, J. E.; Antia, R. Why Are CD8 T Cell Epitopes of Human Influenza A Virus Conserved? *J. Virol.* **2019**, *93*, No. e01534.
(74) Grant, E.; Wu, C.; Chan, K. F.; Eckle, S.; Bharadwaj, M.; Zou, Q. M.; Kedzierska, K.; Chen, W. Nucleoprotein of Influenza A Virus Is a Major Target of Immunodominant CD8+ T-Cell Responses. *Immunol. Cell Biol.* **2013**, *91*, 184−194.
(75) Grant, E. J.; Quinones-Parra, S. M.; Clemens, E. B.; Kedzierska, K. Human Influenza Viruses and CD8(+) T Cell Responses. *Curr. Opin. Virol.* **2016**, *16*, 132−142.
(76) Sridhar, S.; Begom, S.; Bermingham, A.; Hoschler, K.; Adamson, W.; Carman, W.; Bean, T.; Barclay, W.; Deeks, J. J.; Lalvani, A. Cellular Immune Correlates of Protection against Symptomatic Pandemic Influenza. *Nat. Med.* **2013**, *19*, 1305−1312.
(77) McMichael, A. J.; Gotch, F. M.; Noble, G. R.; Beare, P. A. Cytotoxic T-Cell Immunity to Influenza. *N. Engl. J. Med.* **1983**, *309*, 13−17.
(78) Townsend, A. R.; Rothbard, J.; Gotch, F. M.; Bahadur, G.; Wraith, D.; McMichael, A. J. The Epitopes of Influenza Nucleoprotein Recognized by Cytotoxic T Lymphocytes Can Be Defined with Short Synthetic Peptides. *Cell* **1986**, *44*, 959−968.
(79) Lopes, P. P.; Todorov, G.; Pham, T. T.; Nesburn, A. B.; Bahraoui, E.; BenMohamed, L. Laser Adjuvant-Assisted Peptide Vaccine Promotes Skin Mobilization of Dendritic Cells and Enhances Protective CD8(+) Tem and Trm Cell Responses against Herpesvirus Infection and Disease. *J. Virol.* **2018**, *92*, No. e02156-17.
(80) Morabito, K. M.; Ruckwardt, T. R.; Redwood, A. J.; Moin, S. M.; Price, D. A.; Graham, B. S. Intranasal Administration of RSV Antigen-Expressing MCMV Elicits Robust Tissue-Resident Effector and Effector Memory CD8(+) T Cells in the Lung. *Mucosal Immunol.* **2017**, *10*, 545−554.
(81) Shin, H.; Iwasaki, A. A Vaccine Strategy That Protects against Genital Herpes by Establishing Local Memory T Cells. *Nature* **2012**, *491*, 463−467.
(82) Fernandez-Ruiz, D.; Ng, W. Y.; Holz, L. E.; Ma, J. Z.; Zaid, A.; Wong, Y. C.; Lau, L. S.; Mollard, V.; Cozijnsen, A.; Collins, N.; Li, J.; Davey, G. M.; Kato, Y.; Devi, S.; Skandari, R.; Pauley, M.; Manton, J. H.; Godfrey, D. I.; Braun, A.; Tay, S. S.; et al. Liver-Resident Memory CD8(+) T Cells Form a Front-Line Defense against Malaria Liver-Stage Infection. *Immunity* **2016**, *45*, 889−902.
(83) Lee, Y. T.; Suarez-Ramirez, J. E.; Wu, T.; Redman, J. M.; Bouchard, K.; Hadley, G. A.; Cauley, L. S. Environmental and Antigen Receptor-Derived Signals Support Sustained Surveillance of the Lungs by Pathogen-Specific Cytotoxic T Lymphocytes. *J. Virol.* **2011**, *85*, 4085−4094.
(84) Zammit, D. J.; Turner, D. L.; Klonowski, K. D.; Lefrancois, L.; Cauley, L. S. Residual Antigen Presentation after Influenza Virus Infection Affects CD8 T Cell Activation and Migration. *Immunity* **2006**, *24*, 439−449.
(85) Alpar, H. O.; Somavarapu, S.; Atuah, K. N.; Bramwell, V. W. Biodegradable Mucoadhesive Particulates for Nasal and Pulmonary Antigen and DNA Delivery. *Adv. Drug Delivery Rev.* **2005**, *57*, 411−430.
(86) Joffre, O. P.; Segura, E.; Savina, A.; Amigorena, S. Cross-Presentation by Dendritic Cells. *Nat. Rev. Immunol.* **2012**, *12*, 557−569.
(87) Griffiths, K. L.; Ahmed, M.; Das, S.; Gopal, R.; Horne, W.; Connell, T. D.; Moynihan, K. D.; Kolls, J. K.; Irvine, D. J.; Artyomov, M. N.; Rangel-Moreno, J.; Khader, S. A. Targeting Dendritic Cells to Accelerate T-Cell Activation Overcomes a Bottleneck in Tuberculosis Vaccine Efficacy. *Nat. Commun.* **2016**, *7*, 13894.
(88) Beauchamp, N. M.; Yammani, R. D.; Alexander-Miller, M. A. CD8Marks a Subpopulation of Lung-Derived Dendritic Cells with

DOI: 10.1021/acsnano.9b00326
ACS Nano 2019, 13, 10939−10960

Differential Responsiveness to Viral Infection and Toll-Like Receptor Stimulation. *J. Virol.* **2012**, *86*, 10640−10650.
(89) Lee, Y. N.; Lee, Y. T.; Kim, M. C.; Gewirtz, A. T.; Kang, S. M. A Novel Vaccination Strategy Mediating the Induction of Lung-Resident Memory CD8 T Cells Confers Heterosubtypic Immunity against Future Pandemic Influenza Virus. *J. Immunol.* **2016**, *196*, 2637−2645.
(90) Beura, L. K.; Rosato, P. C.; Masopust, D. Implications of Resident Memory T Cells for Transplantation. *Am. J. Transplant.* **2017**, *17*, 1167−1175.
(91) Mueller, S. N.; Mackay, L. K. Tissue-Resident Memory T Cells: Local Specialists in Immune Defence. *Nat. Rev. Immunol.* **2016**, *16*, 79−89.
(92) Shane, H. L.; Klonowski, K. D. Every Breath You Take: The Impact of Environment on Resident Memory CD8 T Cells in the Lung. *Front. Immunol.* **2014**, *5*, 320.
(93) Bergsbaken, T.; Bevan, M. J. Proinflammatory Microenvironments within the Intestine Regulate the Differentiation of Tissue-Resident CD8(+) T Cells Responding to Infection. *Nat. Immunol.* **2015**, *16*, 406−414.
(94) Takamura, S. Niches for the Long-Term Maintenance of Tissue-Resident Memory T Cells. *Front. Immunol.* **2018**, *9*, 1214.
(95) Perrier, S. 50th Anniversary Perspective: Raft Polymerization—a User Guide. *Macromolecules* **2017**, *50*, 7433−7447.
(96) Sevimli, S.; Knight, F. C.; Gilchuk, P.; Joyce, S.; Wilson, J. T. Fatty Acid-Mimetic Micelles for Dual Delivery of Antigens and Imidazoquinoline Adjuvants. *ACS Biomater. Sci. Eng.* **2017**, *3*, 179−194.
(97) Convertine, A. J.; Diab, C.; Prieve, M.; Paschal, A.; Hoffman, A. S.; Johnson, P. H.; Stayton, P. S. pH-Responsive Polymeric Micelle Carriers for SiRNA Drugs. *Biomacromolecules* **2010**, *11*, 2904−2911.
(98) Jacobson, M. E.; Wang-Bishop, L.; Becker, K. W.; Wilson, J. T. Delivery of 5′-Triphosphate RNA with Endosomolytic Nanoparticles Potently Activates RIG-I to Improve Cancer Immunotherapy. *Biomater. Sci.* **2019**, *7*, 547−559.
(99) Murthy, N.; Robichaud, J. R.; Tirrell, D. A.; Stayton, P. S.; Hoffman, A. S. The Design and Synthesis of Polymers for Eukaryotic Membrane Disruption. *J. Controlled Release* **1999**, *61*, 137−143.
(100) Miller, M. A.; Stabenow, J. M.; Parvathareddy, J.; Wodowski, A. J.; Fabrizio, T. P.; Bina, X. R.; Zalduondo, L.; Bina, J. E. Visualization of Murine Intranasal Dosing Efficiency Using Luminescent Francisella Tularensis: Effect of Instillation Volume and Form of Anesthesia. *PLoS One* **2012**, *7*, No. e31359.
(101) Gilchuk, P.; Knight, F. C.; Wilson, J. T.; Joyce, S. Eliciting Epitope-Specific CD8+ T Cell Response by Immunization with Microbial Protein Antigens Formulated with Alpha-Galactosylceramide: Theory, Practice, and Protocols. *Methods Mol. Biol.* **2017**, *1494*, 321−352.
(102) Rodenko, B.; Toebes, M.; Hadrup, S. R.; van Esch, W. J.; Molenaar, A. M.; Schumacher, T. N.; Ovaa, H. Generation of Peptide-MHC Class I Complexes through UV-Mediated Ligand Exchange. *Nat. Protoc.* **2006**, *1*, 1120−1132.

DOI: 10.1021/acsnano.9b00326
ACS Nano 2019, 13, 10939−10960